Journal of Zhejiang University-SCIENCE A (Applied Physics & Engineering) *2024 25(10):765-787*
www.jzus.zju.edu.cn; www.springer.com/journal/11582
E-mail: jzus_a@zju.edu.cn

Review

https://doi.org/10.1631/jzus.A2400139

Time-dependent diffusion magnetic resonance imaging: measurement, modeling, and applications

Ruicheng BA, Liyi KANG, Dan WU✉

Key Laboratory for Biomedical Engineering of Ministry of Education, Department of Biomedical Engineering, College of Biomedical Engineering & Instrument Science, Zhejiang University, Hangzhou 310027, China

Abstract: Increasingly, attention is being directed towards time-dependent diffusion magnetic resonance imaging (TDDMRI), a method that reveals time-related changes in the diffusional behavior of water molecules in biological tissues, thereby enabling us to probe related microstructure events. With ongoing improvements in hardware and advanced pulse sequences, significant progress has been made in applying TDDMRI to clinical research. The development of accurate mathematical models and computational methods has bolstered theoretical support for TDDMRI and elevated our understanding of molecular diffusion. In this review, we introduce the concept and basic physics of TDDMRI, and then focus on the measurement strategies and modeling approaches in short- and long-diffusion-time domains. Finally, we discuss the challenges in this field, including the requirement for efficient scanning and data processing technologies, the development of more precise models depicting time-dependent molecular diffusion, and critical clinical applications.

Key words: Time-dependent diffusion; Diffusion magnetic resonance imaging (dMRI); Microstructure imaging; Microstructural model

1 Introduction

Diffusion magnetic resonance imaging (dMRI) is a promising "super resolution" technology widely used in preclinical and clinical research, which probes the microstructure of tissues by measuring the diffusion behavior of water in different microenvironments and enables non-invasive depiction of voxel averaged information of biological tissues at the cellular scale.

Time-dependency is a fundamental characteristic of the diffusion behavior of water molecules in biological tissues. The diffusion process is significantly influenced by cellular and subcellular structures. During short diffusion times, the diffusion distance is limited and the molecules hardly encounter tissue structures, behaving more as if in free diffusion. However, as the diffusion time increases, the diffusion distance also increases, leading to a higher likelihood of water molecules interacting with obstacles within the tissue. When the diffusion time is sufficiently long, the molecules become restricted within a compartment or move by exchange from the initial compartment to another. These effects are reflected in magnetic resonance imaging (MRI) signals, manifested as diffusion signal values positively correlated with diffusion time due to restriction in short timeframes, and approaching a negative correlation with diffusion time near the long-time limit due to exchange. It is important to note that with increasing diffusion time, the signal becomes more coarse-grained, resulting in the loss of microstructural details that reflect specific shapes, while the proportion of information representing global characteristics increases (Lemberskiy et al., 2017a; Reynaud, 2017; Novikov et al., 2019; Xu, 2021; Wu et al., 2024).

To more accurately describe and quantify the time-dependent characteristics of molecular diffusion, researchers have proposed a series of mathematical models and computational methods (Kärger, 1985; Kärger et al., 1988; Novikov and Kiselev, 2011; Novikov et al., 2011, 2014; Panagiotaki et al., 2014; Jiang et al., 2016; Reynaud et al., 2016; Jelescu et al.,

✉ Dan WU, danwu.bme@zju.edu.cn
Ruicheng BA, https://orcid.org/0000-0003-0475-8225
Dan WU, https://orcid.org/0000-0002-9303-5821

Received Mar. 11, 2024; Revision accepted June 2, 2024;
Crosschecked July 7, 2024; Online first Aug. 22, 2024

2022; Olesen et al., 2022; Gardier et al., 2023). These models and methods not only provide strong theoretical support for time-dependent diffusion magnetic resonance imaging (TDDMRI) but also bring our understanding of molecular diffusion to a new level, forming the basis of the TDDMRI technique. The models mentioned in this review are listed in Table 1.

TDDMRI has received increasing attention in recent years. It reveals changes in the diffusion behavior of molecules over time, allowing us to understand and reconstruct this complex biological process. The technique requires a series of time-series dMRI signals, which are decoupled to extract microstructural information by modeling the dMRI signal as a function of time, diffusion weighting, and microstructural parameters. Modern dMRI is based mainly on a two-dimensional parameter space (q-t space) of diffusion weighting and diffusion time (Burcaw et al., 2015). Previous studies have focused mainly on exploring the q-space as extensively as possible within clinical constraints, akin to observing the details of static samples with higher magnification and more orientations using a microscope. Recently, there has been a shift towards t-space-based research, which concentrates on discovering features by observing the dynamic changes of samples. This distinction represents a pivotal difference between these two categories of studies. However, it is essential to recognize that research within the q-t space is not disjointed: studies in the t-space also necessitate diffusion weighting to some extent. Thus, the TDDMRI used in this study includes dMRI encoding that varies diffusion time with or without changed diffusion weightings, and strongly relies on the time-dependency.

Several efforts have been made to develop improved hardware and optimize advanced sequences to address the challenges of clinical transformation (Xu, 2021; Wu et al., 2024), and TDDMRI has become a vital tool in clinical experiments. Specifically, TDDMRI is used extensively in the preclinical investigation of animal models pertaining to tumors (Panagiotaki et al., 2014; Jiang et al., 2016, 2017, 2019, 2020b, 2024; Reynaud et al., 2016), brain diseases (Novikov et al., 2014; Lee et al., 2020b), and other diseases (Novikov et al., 2011; Winters et al., 2018), thereby contributing substantially to foundational research in these fields. Clinically, TDDMRI has improved our understanding of disease pathophysiology, such as changes in cell size and permeability during tumor progression, and has refined diagnostic approaches. It has also shown promise in early tumor detection and neurological disease assessment by enhancing diagnostic accuracy (Panagiotaki et al., 2015; Fieremans et al., 2017; Xu et al., 2020; Lemberskiy et al., 2021; Zhang et al., 2021; Solomon et al., 2023). In summary, though still in the early stages of clinical translation, TDDMRI has shown significant utility across various disease models and diagnostic applications.

Despite these crucial developments in TDDMRI research, we still face many challenges. In the iteration of hardware and acquisition schemes, we need to

Table 1 Summary of existing signal models mentioned in this review

Model	Acquisition	Status of application	First proposed
POMACE	OGSE, PGSE	Animal model in vivo and in vitro	Reynaud et al., 2016
IMPULSED	OGSE, PGSE	Simulation, cell, animal in vivo, human in vivo	Jiang et al., 2017
VERDICT	PGSE	Cell, animal in vivo, human in vivo	Panagiotaki et al., 2014
rVERDICT	PGSE	Human in vivo	Palombo et al., 2023
SSIFT	OGSE, PGSE	Simulation, cell, animal in vivo, human in vivo	Devan et al., 2022
OGSE ActiveAx	OGSE	Simulation, animal tissue model	Kakkar et al., 2018
Power law	OGSE, PGSE	Simulation, cell, animal in vivo, human in vivo	Novikov et al., 2014
RPBM	STEAM	Simulation, tissue, animal in vivo, human in vivo	Novikov et al., 2011
Karger model	PGSE	Simulation, cell, animal in vivo, human in vivo	Kärger, 1985
TDKI	STEAM	Simulation, phantom, animal in vivo, human in vivo	Jensen et al., 2005
JOINT	OGSE, PGSE	Simulation, cell, animal in vivo, human in vivo	Jiang et al., 2022
NEXI	PGSE	Simulation, animal in vivo	Jelescu et al., 2022
CEXI	PGSE	Simulation	Gardier et al., 2023

POMACE: pulsed and oscillating gradient MRI for assessment of cell size and extracellular space; SSIFT: selective size imaging using filters via diffusion times; RPBM: random permeable barrier model; TDKI: time-dependent diffusion kurtosis imaging; NEXI: neurite exchange imaging; CEXI: cellular exchange imaging; OGSE: oscillating gradient spin echo; PGSE: pulsed gradient spin echo; STEAM: stimulated echo acquisition mode

develop more efficient scanning and data processing technologies to improve the quality and efficiency of imaging. As for research on theory and methodology, we need to propose more scientific and accurate models to describe and quantify the time-dependent behavior of molecular diffusion. In clinical applications, we should strive to develop more clinical application scenarios to translate this technology from basic research to clinical applications. Besides, the broader clinical application of TDDMRI necessitates multi-center studies, which have yet to be conducted.

In this review, we focus mainly on the two extreme time domains: short diffusion time and infinitely long diffusion time. The short-time domain captures insights into constrained microstructural information, while the long-time domain reflects the transmembrane water exchange in the diffusion process. Note that some models may simultaneously use assumptions from both time domains. In this review, we classify models based on the types of parameters they mainly focus on. We first introduce the physical picture of water molecules diffusing in these two domains and define the division of long- and short-time domains. We then discuss the primary sequence protocols used in the two time domains and detail some widely used analytical and microstructure modelling imaging methods, as well as the application of these methods and models to various tissues and diseases. Some views on possible future directions of time-dependent diffusion technology are also presented.

2 Concept and fundamental issues

The diffusion time t_d plays an important role in restricted diffusion systems, and dMRI signals vary with t_d (Stejskal and Tanner, 1965). Typical diffusion measurements are more sensitive to length scale $L(t)$ related to the root-mean-square displacement of diffusion $\langle x^2(t)\rangle$, i.e., $L(t_d)=\sqrt{\langle x^2(t_d)\rangle}=\sqrt{2dDt_d}$, where d represents the diffusion dimension, and D symbolizes the diffusion coefficient. As t_d increases, water molecules coarsen the underlying microscopic structure on an increasing length scale $L(t_d)$. When $L(t_d)\to\infty$, the medium becomes completely homogeneous, yielding the asymptotic diffusion coefficient D_∞ being constant. Thus, the effective diffusion will exhibit different forms as diffusion time increases, as shown in Fig. 1. Due to

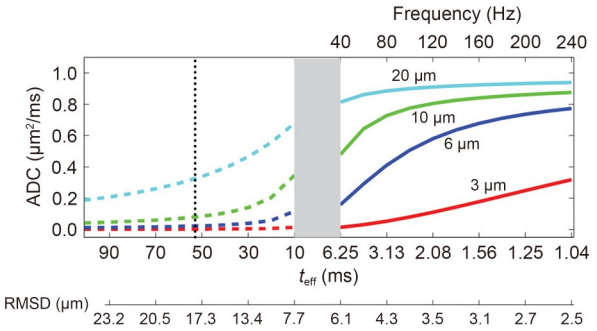

Fig. 1 Relationship between effective diffusion time (t_{eff}) and root mean square displacement (RMSD) in time-dependent diffusion, along with an example of time-dependent diffusion: diffusion spectra quantified with apparent diffusion coefficient (ADC) of restricted water diffusion inside impermeable spheres with diameters of 3, 6, 10, and 20 μm. The gray band divides the spectrum into two regions, representing the readily accessible spectral ranges for PGSE (left) and OGSE (right) methods, respectively. Reprinted from (Jiang et al., 2016), Copyright 2016, with permission from John Wiley and Sons

the complexity and heterogeneity of biological tissues, it is impossible to describe the whole evolution process of $D(t_d)$ or $L(t_d)$ using mathematical formulas. However, we can obtain analytic solutions for extreme cases, resulting in approximate expressions of diffusion signals and diffusion coefficients under specific conditions. Generally, the tissue characteristic diffusion time $t_c\sim R^2/D$ serves as the boundary, where R is the restriction size of the tissue. If $t_d\ll t_c$, it is considered a measurement in the short-time regime, whereas if $t_d\gg t_c$, it is considered a measurement in the long-time domain or approaches the tortuosity limit situation. In practical applications, the typical constraints on t_d tend to be less than or equal to t_c for a short-time regime and an-order higher than t_c for a long-time regime. Note that short- or long-time regime categorization is a relative concept, as the t_c values are quite different in various microstructures. Most thin nerve fibers in humans were found to be shorter than 2 μm (Saliani et al., 2017). Given radial diffusivity of around 1.5 μm²/ms (Lee et al., 2020a), a typical short-time regime is of the order of a few milliseconds according to the equation $t_c\sim R^2/D$, whereas the size of tumor cells generally varies between 10 and 20 μm (Hao et al., 2018), corresponding to a short-time regime in the range of tens of milliseconds. Therefore, our subsequent division of the long- and short-time regimes was based solely on the relative size of t_d compared to t_c, rather than comparing it to a fixed time value.

3 Measurement strategies

3.1 Measurement in the short-time regime

The sensitivity to tissue microstructure depends on the applied gradient waveform for acquiring dMRI data. Measurements in the short-time regime generally apply the oscillating gradient spin echo (OGSE) sequence (Stejskal and Tanner, 1965; Mitra et al., 1992; Schachter et al., 2000), which replaces oscillating gradients with pulsed gradients (Fig. 2a), thereby achieving a shorter diffusion time under hardware limitations. The higher the oscillation frequency of OGSE, the shorter the achievable diffusion time. It is generally considered that the frequency f is related to the effective diffusion time t_{eff} according to $t_{eff}=1/(4f)$ (Parsons et al., 2003; Baron and Beaulieu, 2014; Xu et al., 2014). However, some research suggests this relationship might not be accurate (Lemberskiy et al., 2017b; Xu, 2021). Early OGSE imaging research used sine or cosine modulated gradient waveforms. To ensure a concentrated sampling frequency and achieve high b values at a certain maximum gradient amplitude, cosine modulated trapezoidal waves (commonly referred to as cosine trapezoidal waves) (Van et al., 2014) were introduced and have been widely used in almost all recent human OGSE imaging studies (Gore et al., 2010; Xu, 2021). On standard clinical MRI systems (with maximum gradient G_{max}=80 mT/m and maximum slew rate $R_{s,max}$=200 T/(m·s)), the realizable OGSE is generally f=50 Hz and b=500 s/mm^2. Recent preliminary measurements of OGSE using MAGNUS yielded f=105 Hz and b=1000 s/mm^2 with G_{max}=200 mT/m and $R_{s,max}$=500 T/(m·s) (Foo et al., 2020; Tan et al., 2020).

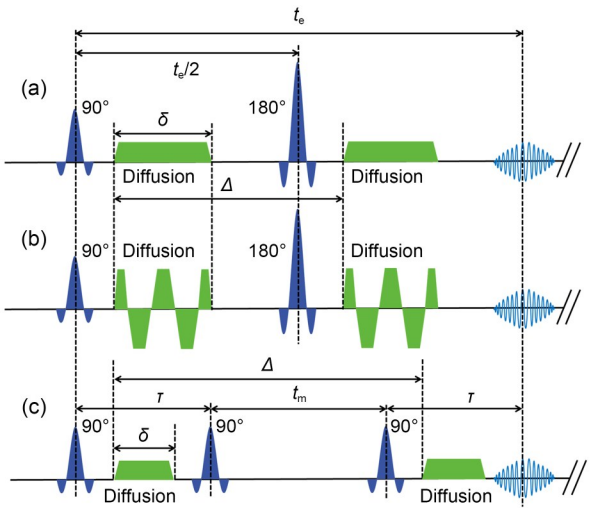

Fig. 2 Waveform of (a) PGSE, (b) OGSE, and (c) STEAM protocol. t_e: echo time; $\tau=t_e/2$

3.2 Measurement in the long-time regime

For long-time regime measurements, the pulsed gradient spin echo (PGSE) sequence (Stejskal and Tanner, 1965) is widely applied for diffusion encoding due to its efficient diffusion weighting. This method uses two pulse diffusion gradients, each with a duration of δ and an interval time of Δ (Fig. 2b). The effective diffusion time is generally represented as $t_{eff}=\Delta-\delta/3$ (Stejskal and Tanner, 1965). In human MRI systems, due to hardware limitations, PGSE is capable of achieving only relatively long diffusion times (e.g., t_{eff}=20–100 ms) (Clark et al., 2001; Grussu et al., 2019; Lee et al., 2020b). Furthermore, the T2 relaxation in the spin-echo measurements at relatively long echo times greatly reduces the signal-to-noise ratio (SNR). Stimulated echo acquisition mode (STEAM) sequence (Merboldt et al., 1991) is also used for TDDMRI. The waveform is shown in Fig. 2c. After applying diffusion gradients, a third 90° pulse is applied to store the signal on the longitudinal plane. After a mixing time t_m, another 90° pulse returns the longitudinal pulse to the transverse plane, thus eliminating signal T2 decay during the diffusion time. This effectively renders a more extended diffusion time and improves sensitivity to longer diffusion times (e.g., t_{eff}=100–800 ms) (Zhang et al., 2021; Solomon et al., 2023). However, diffusion-weighted STEAM (DW-STEAM) leads to a reduction in signal by half, resulting in a lower SNR compared to traditional sequences (Kleinnijenhuis et al., 2018; Solomon et al., 2023).

These sequences were developed to capture the diffusion characteristics of microstructures in the short- and long-time regimes (e.g., restriction and exchange). Recently, novel waveforms, such as free gradient waveforms, have been proposed, allowing the selection of suitable models for the highest contrast based on the research purpose (Chakwizira et al., 2023). Several studies have combined the long- and short-time domain forms (Novikov et al., 2011; Jiang et al., 2016, 2017, 2019, 2021, 2022; Reynaud et al., 2016; Johnston et al., 2019). Reports suggest that the combination of high-frequency and low-frequency OGSEs with standard PGSE gradients can achieve higher microstructural detection sensitivity (Xu et al., 2012, 2014). For biological tissues of changeable scales, the concepts of

long- and short-time regimes are relative; therefore, it is essential to choose appropriate measurement scales and sequence protocols based on the observed structure's characteristics when measuring different tissues.

4 Simulation results and discussion

4.1 Diffusion in the short-diffusion-time regime

4.1.1 Physical picture: behavior of water molecules diffusing in the short-time regime

During the diffusion process in biological tissues, water molecules will continuously encounter barriers that limit or hinder diffusion. These restrictions or obstacles reflect the microscopic structure of the tissues, such as cell size and volume fraction, which in turn provide an opportunity for non-invasive exploration of tissue status. The progression of many diseases is often accompanied by alterations in cellular or subcellular microstructural characteristics. For example, differences are apparent in cell density and cell size between the substance, edema, and necrotic area of tumors and normal tissues. Neurological swelling caused by hypoxia and ischemia (Warach et al., 1995), astrocytic edema and morphological changes like bead-like formations (Budde and Frank, 2010), as well as alterations induced by mechanical pressure on the tissue are features of certain diseases (Hattori et al., 2011). Information reflected by the short diffusion time might offer greater sensitivity for detecting disease progression. Therefore, the short diffusion time provides powerful candidate indicators for the specific and non-invasive description of the cellular structural features of brain neurons, various tissue cells, and tumor cells.

4.1.1.1 Signal and ADC contrast

Many diseases can impact tissues at the cellular and subcellular scales, but alterations can be obscured by the coarse-graining effect of long diffusion times (Novikov et al., 2019). It is evident that the short-time domain signal, typically obtained by OGSE, is different from the signal measured by PGSE and contains different microstructural information. The apparent diffusion coefficient (ADC) is a critical metric of dMRI, reflecting comprehensive cellular-level information. However, in tissues, the ADC is expected to vary with the change of b value (decreasing with increasing b value) and diffusion time (increasing for short diffusion times), and the changes of ADC over time (ΔADC) caused by the time-dependence of diffusion can also reflect additional microstructural information. Common indicators include a direct comparison between ADC_{OGSE} and ADC_{PGSE}, change in ADC (cADC=$ADC_{OGSE}-ADC_{PGSE}$ or ΔADC), or relative change in ADC (rcADC=$(ADC_{OGSE}-ADC_{PGSE})/ADC_{OGSE}$). As one of the earliest attempts to interpret ADC, diffusion tensor imaging (DTI) provides reliable microstructural indicators. The application of OGSE enables DTI to acquire new information at smaller scales hitherto unseen in typical PGSE imaging (Clark et al., 2001; Xu, 2021).

The differential diagnosis and treatment of tumors, especially brain tumors, continue to be a hot research area in medicine. In recent years, researchers have discovered that shorter diffusion times can yield a higher diffusion signal contrast or ADC differentials, providing a non-invasive method for distinguishing between benign and malignant tumors, tumors and normal tissues, and different types of tumors (Colvin et al., 2008, 2011; Xu et al., 2012; Bongers et al., 2018; Iima et al., 2019; Zhu et al., 2023). Several mouse tumor model studies found that the tumor ADC measured by PGSE at typical diffusion times did not significantly differ from that of normal tissue, whereas the tumor ADC measured by short-diffusion-time OGSE was higher than that of the surrounding tissue, enhancing the contrast between tumor and normal tissue regions. Moreover, ADC_{OGSE} significantly increased during radiation and chemotherapy, corresponding to a response to treatment (Colvin et al., 2011; Xu et al., 2012; Bongers et al., 2018). These findings aligned with the results of human scan studies of various conditions such as head and neck tumors, brain gliomas, and prostate tumors (Lemberskiy et al., 2017a, 2018; Iima et al., 2019; Zhu et al., 2023).

In addition, some studies have reported that malignant tumors exhibit more significant ADC differentials compared to benign tumors, which suggests the possibility of using ΔADC to determine the malignancy of tumors. Kamimura et al. (2023a) conducted a retrospective human study and successfully used ΔADC to distinguish between glioblastoma and brain metastasis in the enhanced region ($p<0.01$), significantly surpassing the conventional ADC0Hz method in terms of area under curve (AUC) ($AUC_{\Delta ADC}=0.877$, $AUC_{ADC0Hz}=0.595$, $p<0.001$). Maekawa et al. (2019) found that ADC values measured by OGSE (t_{eff}=6.5 ms) and PGSE (t_{eff}=35.2 ms) were lower in choroid plexus cysts than in

cerebrospinal fluid under short diffusion times, indicating restricted spatial diffusion and increased cystic viscosity. For non-axial brain tumors, high-grade tumors had higher ΔADC(max) and rcADC(max) values for ADC absolute differences in OGSE and PGSE measurements than low-grade tumors (p<0.01), while the ΔADC(max) values for normal white matter were lower than those for high-grade and low-grade brain tumors (Maekawa et al., 2020). Non-axial brain tumor studies showed that compared to meningiomas (ΔADC=15.7, ±4.4%) and auditory nerves (ΔADC=12.4, ±8.2%), pituitary adenomas (ΔADC=46.8, ±11.3%) had the highest average (standard deviation) relative percentage change in ADC, i.e., they showed a stronger diffusion time dependency (Maekawa et al., 2023).

In addition to brain tumors, studies on hepatocellular carcinoma (Wagner et al., 2020) and breast cancer (Someya et al., 2022) have also shown greater temporal changes in ADC in the pericancerous area. Malignant tumors have higher ΔADC values than benign tumors (Iima et al., 2020a), and the ΔADC performance in different molecular types of breast cancer also differs (Iima et al., 2021).

Another major use for short-diffusion-time diagnostics is in strokes. As a sensitive method for diagnosing stroke, dMRI has been widely applied, and it has been reported that the contrast between ischemic lesions and normal tissue decreases with shorter diffusion times (Baron et al., 2015; Boonrod et al., 2018). Given PGSE's high sensitivity to stroke, short-diffusion-time OGSE imaging might not replace stroke diagnosis, but could provide new insights into stroke lesions (Xu, 2021). The difference in signal contrast between short and long diffusion times potentially results from stroke-related occurrences such as neural beading and axonal swelling (Warach et al., 1995; Budde and Frank, 2010; Baron et al., 2015; Boonrod et al., 2018). Simulations and animal experiments have shown that ADC measurements from high-frequency OGSE can provide differences in contrast between cell layers (Aggarwal et al., 2012; Wu et al., 2014); cADC was significantly higher in the ipsilateral region of oxygen-glucose deprivation damaged brains, potentially indicating sensitivity to subcellular structures (Aggarwal et al., 2014; Wu et al., 2014, 2019), a result confirmed by human experiments (Gao et al., 2021; Xu, 2021).

In addition, the signal contrast brought about by shorter diffusion times, direct comparison between ADC_{OGSE} and ADC_{PGSE}, as well as the change in ADC values have provided new insights into the microstructural differences between different brain tissue structures (Grussu et al., 2019; Foo et al., 2020), and diagnoses of diseases such as normal pressure hydrocephalus (NPH), epidermoid cyst, multiple sclerosis, and Duchenne muscular dystrophy (McDowell et al., 2021; Xu, 2021). Fig. 3 shows the ADC_{OGSE} and ADC_{PGSE} maps in different diseases. In animal and human experiments, OGSE DTI studies have consistently found that shorter diffusion times lead to significant increases in DTI eigenvalues of grey matter, and declines in the fractional anisotropy (FA) of white matter (Kershaw et al., 2013; Baron and Beaulieu, 2014). In one animal

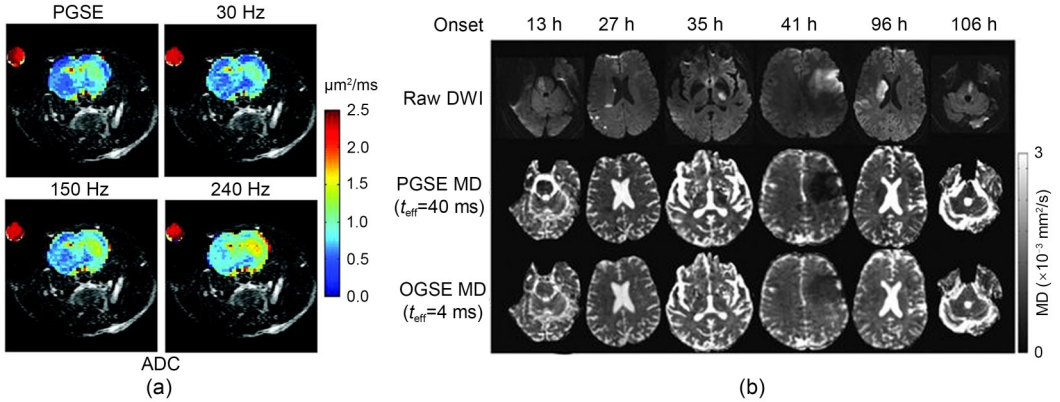

Fig. 3 (a) Color ADC maps of rat brain tissue inoculated with glioblastoma cells (a smaller t_d provides an increased contrast and shows more spatial heterogeneity inside brain tumors) (reprinted from (Colvin et al., 2008), Copyright 2008, with permission from American Chemical Society); (b) Images of raw DWI, PGSE MD, and OGSE MD of human brain with ischemic stroke (DWI: diffusion-weighted imaging; MD: mean diffusivity) (reprinted from (Baron et al., 2015), Copyright 2015, with permission from Wolters Kluwer Health, Inc.). References to color refer to the online version of this figure

experiment, the frequency dependence of the vertical diffusion rate in the corpus callosum was significantly higher, and high-resolution 3D diffusion tensor images obtained from high-frequency oscillating gradients could be used to distinguish different cellular layers in the brain and cerebellum (Aggarwal et al., 2012). Recently, a study discovered that the time-dependence of diffusion tensor imaging is related to age and gender differences (Tétreault et al., 2020). Frequency-dependent DTI using OGSE in whole-body gradient systems can be used for in vivo human research, but is restricted to relatively low b values and/or oscillation frequencies (i.e., $f_{max}\times b_{max}\leqslant 0.035$ μm^{-2}) (Dai et al., 2023).

Xu et al. (2012) observed competing effects at different length scales in live tissue using dMRI technology, with high-frequency OGSE being more sensitive to subcellular scales and PGSE being more sensitive to cellular scales. The signal expression in the mid-frequency range may be affected by changes in cell density and intracellular structure. Given the complexity and heterogeneity of biological tissues, the settings of t_{eff} (Lemberskiy et al., 2018; Iima et al., 2019; Kamimura et al., 2023b) and the selection of thresholds (Shi et al., 2018) have a significant impact on the classification results based on ΔADC for distinguishing different tumors. Generally, variation brought by different diffusion times shows tremendous potential for distinguishing and diagnosing tumors using ADC values. However, since there is no standardized comparison sequence or ADC/signal intensity threshold for different diseases, differences stemming from different diffusion times are more suitable as auxiliary diagnostic information (Iima et al., 2020a). More quantitative research and long-term clinical validation are still needed to standardize the process of data analysis, improve the accuracy of differentiation, reduce the risk of misdiagnosis, and eventually achieve individualized, precise disease diagnosis and prognosis.

4.1.1.2 Frequency dependence of $D(t)$

Measuring diffusion signals and diffusion metrics over a wide range of frequencies and diffusion times can obtain the diffusion spectrum, which is the ideal parameter for describing the comprehensive information of tissue microstructures (Xu, 2021). If we consider $t\approx 1/\omega$, then at the high-frequency range ($\omega\to\infty$), the equation derived by Mitra et al. (1993) and Parsons et al. (2006) in porous media can be generalized under both PGSE and OGSE as $D(t)\sim\omega^{-1/2}$ (Novikov and Kiselev, 2011; Xu et al., 2011). In the short-time domain, its expression is as follows (Novikov and Kiselev, 2011):

$$D(\omega)\cong D_0\left(1-\frac{4}{3d\sqrt{\pi}}\cdot\frac{S}{V}\sqrt{\frac{D_0}{\omega}}\right),\ D_0\equiv D|_{\omega\to\infty}. \quad (1)$$

The validity of surface-to-volume ratio (S/V) estimates was verified on sedimentary rocks and beads (Reynaud, 2017). Note that studies have shown that although in extremely short diffusion times, subcellular structures such as the cell nucleus may affect the accuracy of the expression, the relative apparent S/V still provides a valuable parameter to describe the microstructure of tissues (Xu et al., 2011; Reynaud et al., 2016). In cellular models, an average ADC dispersion rate in the range 50–250 Hz demonstrated sensitivity to the treatment of colorectal tumor SW620 with barasertib (Reynaud, 2017). In mouse models, high-frequency oscillating gradient images revealed different frequency dependences for different cellular layers (Aggarwal et al., 2012; Wu et al., 2014). For example, in a model of demyelination, structures with high frequency-dependent ADC increases were pronounced in demyelinated mice (Aggarwal et al., 2012).

However, ex vivo experiments performed on kidney and liver tissue showed very little contrast with dispersion rate compared to conventional ADC (Reynaud, 2017).

In humans, the diffusion time required for the spatial scale of human muscle fibers (30–50 μm) is several hundreds of milliseconds, making short-time domain research viable (Novikov et al., 2011). The Mitra mechanism range of human brain fibers may be less than 1 ms, thus requiring frequencies greater than 1 kHz. In clinical MRI systems, due to the limitation of gradient strength, short-diffusion-time mechanisms are often less suitable for detecting the mesoscale structures in biological tissues.

Therefore, the power-law form of the short-time domain is more suitable for reflecting structural features, differentiating between long- and short-time domains, or being applied as a constraint condition in models such as RPBM (Novikov et al., 2011) or POMACE (Reynaud et al., 2016).

4.1.1.3 Frequency dependence of kurtosis value $K(t)$

In addition to the frequency dependence of ADC or DTI eigenvalues, studies have found that kurtosis

values $K(t)$ also show frequency dependence. Numerous simulations and animal experiments have observed the non-monotonic behavior of kurtosis changing with time, increasing in the short-time domain and decreasing in the long-time regime (Aggarwal et al., 2020; Lee et al., 2020b). However, this phenomenon has not yet been observed in human experiments.

Even under the OGSE sequence with the highest frequency of 47.5 Hz, Dai et al. (2023), using the high-performance MAGNUS gradient magnetic resonance imaging system, observed frequency dependence of diffusion rates and kurtosis in both entire and localized white matter (WM) and gray matter (GM) areas of humans, but the kurtosis always showed a decreasing trend over time.

In mouse experiments, Wu et al. (2018) reported that OGSE kurtosis measurements could provide more information about microstructural changes after ischemic stroke. However, due to technical challenges such as the performance of gradient systems, discoveries from simulation and animal studies regarding time/frequency-dependent diffusion MRI have not been fully translated into in vivo human research (Borsos et al., 2023; Dai et al., 2023).

4.1.2 Models and applications

Within the short-time regime, novel insights into the diagnosis of various diseases rely mainly on signal contrast, the time dependence of the signal in the short-time domain, and the quantified biophysical indicators of cell structural features.

Microstructure modeling in the short-time domain typically assumes Gaussian diffusion and simplifies cells into basic geometric structures, such as axonal cells viewed as cylinders, or tumor cells viewed as spheres or hollow spheres. The signal expression measured by the PGSE sequence in simple geometries was first derived by Stejskal and Tanner (1965). Jiang et al. (2016) updated the expression measured using the OGSE sequence, meeting the need for signal analytical expressions at shorter diffusion times. Based on these expressions, there are currently three models that are widely used preclinically or clinically: IMPULSED (Jiang et al., 2017), POMACE (Reynaud et al., 2016), and VERDICT (Panagiotaki et al., 2014).

4.1.2.1 POMACE

The POMACE model is a two-compartment model in the absence of exchange (Reynaud et al., 2016). It measures a high-frequency OGSE to estimate the surface-to-volume ratio and free diffusion rate D_0, and then fittings are made to the model of impermeable spheres soaked in extracellular space (ECS), with low-frequency OGSE and PGSE measurements assessing four model parameters, including ECS, cell radius (R_{cell}), and diffusivities in the intracellular and extracellular spaces (D_{ICS} and D_{ECS}). POMACE is used mainly for tumor models.

In vivo and in vitro experiments on the GL261 glioma mice model showed that the measured ECS matched previous research and correlated well with microscopic optics. Additionally, cell sizes broadly aligned with electron microscope (EM) measurements. However, the high oscillating frequency of OGSE makes clinical translation of POMACE a great challenge (Reynaud, 2017). As yet, there are no cases of POMACE being used in humans.

4.1.2.2 IMPULSED

The IMPULSED model is also a two-compartment model without exchange (Jiang et al., 2017). It collects OGSE measurements at various frequencies and a single PGSE measurement at a relatively long diffusion time. This model quantifies microstructural parameters such as cell size, density, and intercellular and extracellular diffusion coefficients, with a primary focus on size estimation. Its basic form is

$$\frac{S}{S_0}=f_{in}S_{in}(d_s,D_{in})+(1-f_{in})S_{ex}(D_{ex0},\beta), \quad (2)$$

where S_0 is the signal without diffusion weighting, f_{in} is the relaxation-weighted intracellular signal fraction, and S_{in} and S_{ex} are the intercellular and extracellular signals, respectively. S_{in} is modeled by diffusion within spheres of diameter d_s, with intrinsic cytosol diffusivity D_{in}. S_{ex} is modeled as

$$S_{ex}(D_{ex0},\beta)=\exp[-b(D_{ex0}+\beta)], \quad (3)$$

where D_{ex0} is the extracellular diffusion rate at frequencies close to 0, and β is the slope of extracellular diffusion coefficient with respect to frequency f, which contains information on structural dimensions.

The IMPULSED model is applied mainly to brain, breast, and liver tumor models. Initial experiments on mouse erythroleukemia (MEL) and human K562 early granulocytic leukemia cells demonstrated a high

consistency between cell diameters estimated by the model and cell sizes obtained from optical microscopes (Jiang et al., 2017). Jiang et al. (2017) further demonstrated that the IMPULSED model, using a high-frequency f=150 Hz (t_{eff}=1.7 ms) OGSE, low-frequency f=50 Hz (t_{eff}=5.0 ms) OGSE, and PGSE (t_{eff}=46.7 ms) in in vivo tumor models, showed a positive correlation between the histology of tumor cells and IMPULSED-derived cell density (Spearman coefficient is 0.81; p< 0.0001). They also found that using MRI to derive cell size could detect significantly reduced triple-negative breast tumors after treatment (p<0.05). This demonstrated the feasibility of applying the IMPULSED method for deriving quantitative microstructural parameters in preclinical tumor models and its capacity as a biomarker to describe cancer characteristics and prognosis, and to detect radiotherapy responses (Jiang et al., 2017, 2019, 2020b, 2024).

Xu et al. (2020) reported the first application of OGSE imaging in human breast tumors in vivo with t_d ranging from 8.77 to 66.7 ms. They mapped microscopic indicators such as breast tumor cell size, and assessed variation in cell size within tumors of breast cancer patients (Xu et al., 2020). They also reported the first application of OGSE imaging in human livers in vivo with t_d from 2.5 to 38.7 ms (Jiang et al., 2020a). Studies thereafter demonstrated the clinical feasibility of characterizing the cell microstructure using the IMPULSED model. Zhang et al. (2023) measured the IMPULSED signals using OGSE (f=50 and 25 Hz) and PGSE (t_{eff}=30 ms) sequences while limiting the acquisition time to about 4.5 min. Their study showed a good correlation between IMPULSED-derived f_{in} and histological results (r=0.7, p<0.0001) and found that the cell density derived from IMPULSED ($\rho=d_s/(f_{in}\times100)$) had the highest AUC (0.91) in distinguishing high- and low-grade gliomas, outclassing traditional indicators. Ba et al. (2023) also verified that in breast cancer cells, the correlation between IMPULSED-estimated diameter and histological values was very good (r=0.84, p< 0.0001), and the size of breast tumors derived from the IMPULSED model had significance in distinguishing breast tumor molecular subtypes, with estimated d significantly higher than that in the HER2-positive group and LN-positive group (p<0.05) (Fig. 4). They also reported the high requirements of the IMPULSED model in clinical trials for sequence aspects such as minimum diffusion time and SNR.

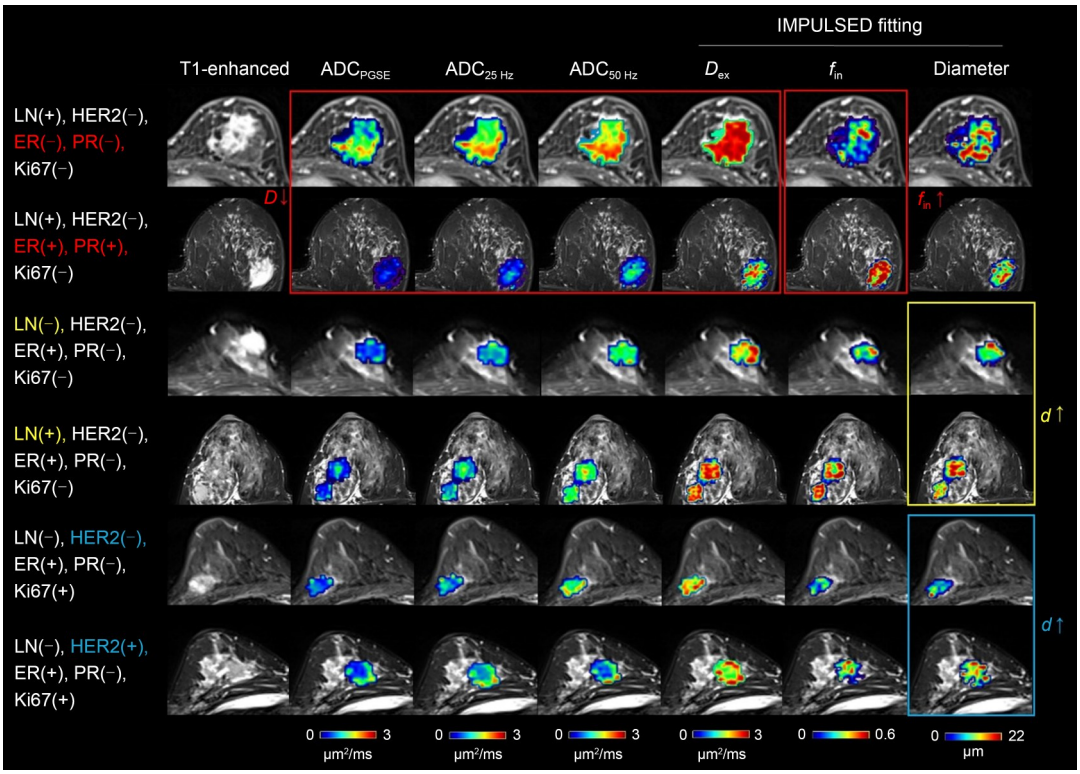

Fig. 4 IMPULSED-derived microstructure properties of breast tumor (for more details refer to Ba et al. (2023)). Reprinted from (Ba et al., 2023), Copyright 2023, with permission from Springer Nature

However, IMPULSED simplifies cancer cells as spheres and assumes that the average cell size derived from the use of IMPULSED includes all cell types (such as cancer cells, matrix cells, and lymphocytes). It is challenging to specifically distinguish between cancer cells and other cells without anticipating the distribution of cell sizes. Refinements to the IMPULSED model would need to consider estimating cell morphology, cell distribution (Xu et al., 2021), membrane permeability (Jiang et al., 2022), modeling of extracellular space (Xu et al., 2023), and the effects of intravoxel incoherent motion (IVIM) and T2 relaxation. The improvements in modeling assumptions and clinical use with temporal diffusion spectroscopy (TDS) to some extent enhance the accuracy and stability of the model. Some researchers are working to improve the stability and accuracy of model fitting in the fitting algorithm to enhance the robustness of fitting under a low SNR (Wu et al., 2023; Liu et al., 2024). However, the microstructural parameters estimated by each model have not been compared clinically, and the effectiveness of the model needs to be more extensively tested.

4.1.2.3 VERDICT

VERDICT is a biophysical, multi-compartment model fitted on DW-MRI measurements (Panagiotaki et al., 2014). This model focuses on diffusion times of t_{eff}=10–40 ms, a timeframe achievable by PGSE sequences, thus making it more suitable for clinical application. The VERDICT model measures PGSE sequences in various directions and at multiple b values. Characteristically, it considers vascular modeling, giving it more parameters and increased complexity. Its basic form is as follows:

$$\frac{S}{S_0}=f_{ic}S_{ic}(d_s,D_i)+f_{EES}S_{EES}(D_e)+f_{vasc}S_{vasc}(D_{vasc}), \quad (4)$$

where D_i, D_e, and D_{vasc} are the intrinsic diffusivities. f_{ic}, f_{EES}, and f_{vasc} are the relaxation-weighted signal fractions (f_{ic}+f_{EES}+f_{vasc}=1) of the intracellular space, extracellular space, and vascular ADCs, respectively, and S_{ic}, S_{EES}, and S_{vasc} are the corresponding signals. In practical applications, several parameters are usually fixed to enhance parameter fitting stability including D_i, D_e, and D_{vasc}.

VERDICT is applied mainly to diseases rich in vascular changes, such as prostate cancer. Its first in vivo application was to quantify and map histologic features of tumors. Results showed that the intracellular volume fraction derived from VERDICT is extremely close to microstructural parameters obtained from histological stained slices, with cell volumes being slightly larger–possibly due to shrinkage during tissue slice preparation. Experimentation on colorectal adenocarcinoma xenografts in mice indicates that different tumors yield significantly different VERDICT-derived intracellular volume fractions, cellular size indices, and pseudo-diffusion coefficients, demonstrating VERDICT's potential for studying tumors on a region-based level and revealing underlying heterogeneity.

Panagiotaki et al. (2015) demonstrated the feasibility of applying VERDICT to prostate cancer in a clinical setting. They found significant increases in estimated f_{ic} and f_{vasc} and a decrease in the f_{EES} (p=0.05) for malignant peripheral zones compared with benign peripheral zones. This finding has been replicated by multiple research groups and inspired more researchers to explore the application of the VERDICT model in prostate cancer (Johnston et al., 2016, 2019; Bailey et al., 2018; Singh et al., 2022).

However, key challenges to VERDICT's clinical application remain, including the specific assumptions about cell structure and substantial signal loss due to relaxation during long spin-echo times. While a discussion has emerged around different modeling approaches for each part concerning the goodness-of-fit of data, the adoption of the ball-ball-sphere (BBS) model for the three compartments may better explain microstructural characteristics of prostate bone metastatic tumors (Bailey et al., 2018), reflecting the need to fine tune model assumptions in various clinical applications. Palombo et al. (2023) developed the relaxation-optimized model (rVERDICT), which provides T1/T2 estimates and microstructural parameters unaffected by tissue relaxation properties. In particular, due to the complexity of VERDICT models, pre-fixed parameters are generally used in clinical use, or more appropriate fitting tools are applied and developed to enhance their clinical feasibility (Fokkinga et al., 2023). Nonetheless, VERDICT requires acquisition optimization for high b values (up to ≈3000 s/mm^2) and various Δ and δ along with potential t_e in its recent extensions, suggesting it still relies on extended acquisition schemes that might be impractical in clinical scenarios with limited scanning time.

4.1.2.4 Other models

In addition to the primary models referenced above, there are other models applicable to brain tumor and cerebral fiber imaging. The SSIFT model (Devan et al., 2022) uses the area encased by signals at different times to distinguish brain tumors from peritumor edema and radiation necrosis due to the model's sensitivity to cell size. Kakkar et al. (2018) suggested that estimates of axon diameter from using OGSE ActiveAx are more accurate and precise than those from using single diffusion encoding (SDE). Herrera et al. (2022) proposed a model for studying human axons with diameters in the 1–2 μm range using OGSE sequences. This model emphasizes the necessity of axonal orientation dispersion, demonstrating closer fitting results than ActiveAx and histological outcomes.

4.2 Diffusion in the long-diffusion-time regime

4.2.1 Physical picture: behavior of water molecules diffusing in the long-time regime

Long-term diffusion approximates the tortuous limit of water molecule diffusion within tissues, leading to a coarse-graining effect (Fig. 5) at the cellular and subcellular scale. Given that the theoretical diffusion distance of water molecules surpasses cell size, the permeability of the cell membrane might emerge as a new index affecting the expression of the diffusion coefficient. On the other hand, local fluctuations in the weak heterogeneous media determine the asymptotic approximation of the diffusion coefficient to the tortuous limit. This provides an angle to noninvasively infer the global diffusion dimension of water molecules and the distribution of tissue structures. Some of these insights include identifying mesoscale structures affecting water diffusion in muscle and brain tissue based on specific values of the dynamic index during MRI measurement, or explicating structural changes underpinning the drop in diffusion coefficient during ischemic stroke (Novikov et al., 2014), and reflecting demyelination levels through changes in membrane permeability (Nedjati-Gilani et al., 2017).

Note that in numerous scenarios, these two mechanisms compete, i.e., water exchange phenomena exist between two compartments undergoing separate coarsening. Several articles have discussed this particular phenomenon (Lee et al., 2020b; Jelescu et al., 2022; Olesen et al., 2022). Lee et al. (2020b) discussed these two situations based on the water exchange time (τ_{ex}). In the long domain, if $t_d \ll \tau_{ex}$, the dominance of structural disorder is considered. If $t_d \cong \tau_{ex}$, the water exchange process plays a dominant role in signal expression.

4.2.2 Models and applications

4.2.2.1 Power law

Mitra et al. (1993) and Parsons et al. (2006) proposed a power-law expression of the time dependence of the internal diffusion coefficient in the short-term

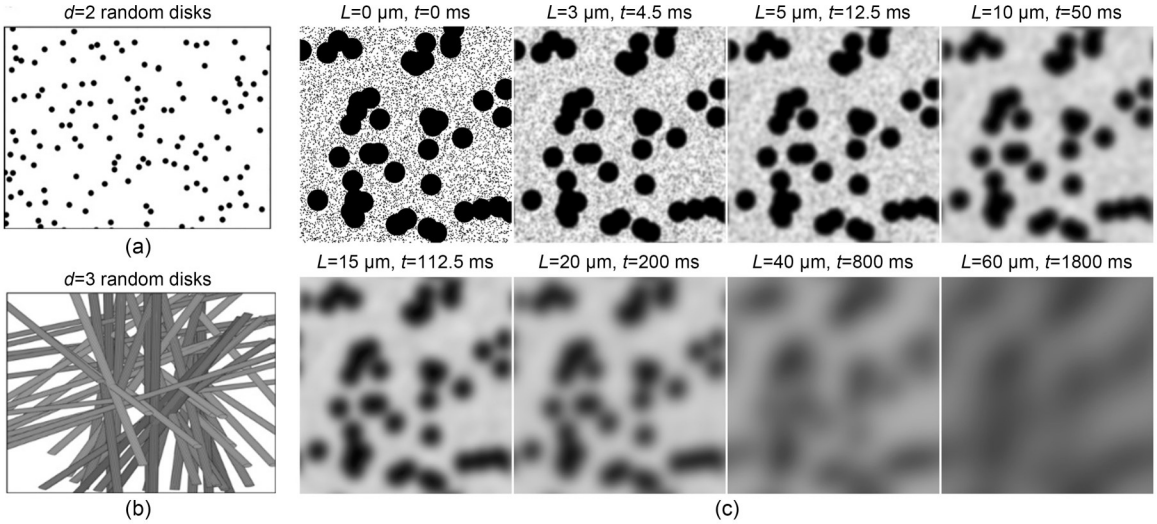

Fig. 5 (a, b) Different structural universality classes in dimensions d=2 and d=3 (reprinted from (Lee et al., 2020b), Copyright 2020, with permission from Springer Nature); (c) Coarse-graining illustrated by the diffusion in a medium where the mesoscopic structure is created by randomly placing black disks of two different radii (reprinted from (Novikov et al., 2018), Copyright 2018, with permission from John Wiley and Sons)

domain. As the diffusion time increases, the power law might be affected by $D(t)\sim t^{-1}$ or higher order quantities (Parsons et al., 2006; Xu et al., 2011). In the tortuous limit, weakly heterogeneous media exhibit local fluctuations, implying perturbative solutions to its diffusion time dependence. Novikov et al. (2014) supported the proposal that the dynamic index of the instantaneous diffusion coefficient $\mathcal{D}(t)$ altering over time can distinguish among universal categories of mesoscopic structural complexity.

$$\mathcal{D}(t)\sim D_\infty + A\cdot t^{-\vartheta},\quad \vartheta=\frac{p+d}{2}, \tag{5}$$

where A is the associated strength of the structural disorder, which is being effectively coarse-grained (Novikov et al., 2019) by the molecules traveling over an increasing diffusion length, and the structural exponent p determines the structural universality class in d spatial dimensions, as shown in Fig. 5. The dynamical exponent ϑ characterizes diffusion in the long-time limit. dMRI typically measures the cumulative diffusion coefficient $D(t)$, which is the time-integrated instantaneous diffusion coefficient $\mathcal{D}(t)$. Therefore, a ϑ greater than 1 would be obscured by 1. The interpretation of ϑ determines the disorder in the placement of restrictions, enabling the identification of their exact source and the selection of the most suitable model based on the measurements. For example, ϑ=1/2 is the signature of a short-range disorder in 1D diffusion, and was observed in both healthy rat brains and those with large-scale ischemia. This indicates the decrease of the diffusivity in lesions is due to structural changes affecting the diffusion along randomly oriented narrow neurites, such as beading (Novikov et al., 2014; Lee et al., 2020b). On the other hand, the slope A reflects the role of disorder, and can be interpreted as changes in restriction properties, though the specific relationship requires further exploration (Lee et al., 2020a). Note that in different measurement directions, the power and slope may vary. For instance, while diffusion along the fiber in fresh ex vivo muscle tissue samples is unrestricted, the transverse components demonstrate dispersion with ϑ=1/2 in 2D diffusion. Therefore, it is crucial to evaluate dispersion effects in the main direction (Novikov et al., 2014; Lee et al., 2020a).

Power laws provide theoretical support for understanding water diffusion patterns in brain, tumor, and muscle tissues. As mentioned above, ϑ=1/2 has been demonstrated in both healthy and globally ischemic rodent brains (Does et al., 2003; Novikov et al., 2014; Wu and Zhang, 2017). Lee et al. (2020b) reported similar power in the cortical gray matter of humans, suggesting that short-range disorder with p=0 in one dimension is a common microscopic characteristic of mammalian neuronal heterogeneity. Specifically, the diffusion in gray matter is dominated by intracellular diffusion, which is hindered mainly by spines and beads along dendrites and axons. The value of ϑ=1/2 was also observed in the structure of mouse leg muscle fibers in the long-time range (Winters et al., 2018), indicating the characteristic of the extended permeable membrane (barrier) disorder class. This corresponds to 2D diffusion occurring between lines drawn at random angles on a plane. In the context of cancer, power-law behavior with ϑ=1 has been reported in prostate cancer. The mean diffusivities in both benign and malignant peripheral zones decrease significantly with time according to a power law (t^{-1}) (p<0.029), while this behavior is not observed in the benign transition zone. This could potentially reveal differences in microstructure characteristics among prostate regions. Additionally, the time dependence of t^{-1} could inform the selection of diffusion times in measurements to maximize the detection of significant differences in tumor grade (Lemberskiy et al., 2017a).

Recent studies have further explored the law. In measurements of both in vivo and in vitro animal experiments using PGSE (considered as 0 Hz) and OGSE (50–250 Hz), Xu et al. (2012) found that ADC had an approximately linear relationship with frequency. Hence, including PGSE as 0 Hz could potentially overshadow the frequency/time dependency of the measured ADC (Van et al., 2014). ϑ=1/2 (Arbabi et al., 2020) and a trend toward ϑ<1 (Baron and Beaulieu, 2014) have been observed in the in vivo human brain using f=0–60 Hz and f=0–50 Hz OGSE. In global white matter and some cortical regions of interest (ROIs), Dai et al. (2023) noted that the kurtosis index (ϑ_K) deviated from 0.5 or 1.0, indicating that in human cortex, the transition time of kurtosis from short-time to long-time limits could be between 14.2 and 21.2 ms, during which a mixed effect of size restriction and water exchange could occur (Lee et al., 2020b; Dai et al., 2023).

4.2.2.2 RPBM

RPBM is a method that does not assume specific cellular geometric shapes. Novikov et al. (2011), who

developed the RPBM model, found the disordered extended restrictions in d=2 dimensions seemed to provide an adequate sketch of a cross-section of myofibers. This method assumes that the muscular membrane is the primary restriction for water movement, typically using STEAM sequences to cover diffusion times from tens to hundreds of milliseconds. RPBM is characterized by three parameters: the free diffusion coefficient D_0, the membrane permeability κ (assumed to be the same for all membranes), and the ratio of membrane surface to volume S/V. Its basic expression is:

$$\mathcal{D}(\omega)=\frac{D_0}{1+\zeta+2z_\omega(1-z_\omega)\left[\sqrt{1+\frac{\zeta}{(1-z_\omega)^2}}\right]},$$
$$z_\omega=\mathrm{i}\sqrt{\mathrm{i}\omega\tau}. \tag{6}$$

It is represented by three parameters D_0, ζ, and z_ω, where the effective "volume fraction" $\zeta=(S/V)/d$ occupied by the membrane (here d denotes the dimension of diffusion), and $\tau=D_0/(2\kappa)^2$. The real part of $\mathcal{D}(\omega)$ is determined by the signal measured by OGSE, while the results of PGSE are used for the fitting of the cumulative diffusion coefficient $D(t)$ (Novikov et al., 2011; Fieremans et al., 2017).

This model is used mainly in muscle tissues and cancer models. A significant correlation between the measured S/V and the perimeter-to-area ratio (P/A) obtained from histology was found in murine leg muscle fibers in vivo (r=0.56, p=0.025) and ex vivo (r=0.71, p=0.01), suggesting a significant correlation in restriction size and revealing that muscle cell size and membrane permeability could be important microstructural indicators of muscle growth (Winters et al., 2018). Some studies in humans that explored the feasibility of clinical applications found that the microstructural markers explained by RPBM could potentially be used to reveal chronic exertional compartment syndrome (Sigmund et al., 2014), calf and shoulder muscle atrophy (Fieremans et al., 2017; Lemberskiy et al., 2021), and other potential insights into pathological changes in muscle tissue. Recently, RPBM was applied to in vivo studies of oropharyngeal squamous cell carcinoma, revealing a strong correlation between tumor S/V and histological results (r=0.47, p=0.014). It was shown to correlate with the clinical staging of oropharyngeal or oral cavity squamous cell carcinomas (OPSCC/OCSCC) and could possibly be used to quantify microstructural parameters and the early response of cancer cells to treatment (Cao et al., 2024).

4.2.2.3 Kärger model

One crucial assumption of most biophysical models within the short-time domain is that water exchange between cells can be neglected, yet this assumption may not hold in the long-time regime (Nilsson et al., 2009; Jelescu et al., 2022). As a result, specific models incorporating intra- and extracellular water exchange should be developed. The most classic model is the two-compartment model with exchange capability, namely the Kärger model (KM) (Kärger, 1985; Kärger et al., 1988). This model assumes that spins of two components occupy space at ratios of f_1 and f_2 respectively, with position-independent exchange occurring. The diffusion coefficients are D_1 and D_2. Coupled Bloch-Torrey equations are used to describe the changes in dual-component magnetic density at any location in space. When the residue times τ_1 and τ_2 of the spins in the two compartments meet the equilibrium condition ($f_1\tau_2=f_2\tau_1=\tau_{ex}$), the equations give a double exponential form of signal attenuation:

$$\frac{M_t}{M_0}=f_1'\mathrm{e}^{-D_1'q^2t}+f_2'\mathrm{e}^{-D_2'q^2t}, \tag{7}$$

where M_t denotes the diffusion-weighted transverse magnetization, and M_0 represents the value without diffusion weighting. The weighted volume fractions (f_1', f_2') and diffusion coefficients (D_1', D_2') are determined together with f_1, f_2, D_1, D_2, τ_1, τ_2, and the diffusion gradient vector $\boldsymbol{q}$.

A number of computer simulations have validated the effectiveness of the KM in the long-time domain and made corrections for the time-dependent restrictions of compartments within KM and the impact of T2 relaxation (Price et al., 1998; Stanisz et al., 1998; Meier et al., 2003; Harkins et al., 2009; Fieremans et al., 2010; Haddar et al., 2016). Results of cell experiments (Andrasko, 1976; Tanner, 1983), animal experiments (Paran et al., 2004; Jespersen et al., 2018; Jelescu et al., 2022; Olesen et al., 2022; Li et al., 2023), and human brain experiments (Nilsson et al., 2009; Lee et al., 2020b; Jelescu et al., 2022) indicate the applicability of KM in the context of red cells, brain white and gray matter, and tumor models, validating its effectiveness in capturing water exchange phenomena. According

to the results based on KM fitting, water exchange in healthy human brain white matter is considered to be at the second or sub-second level, while demyelination leads to a reduction in exchange time (Nedjati-Gilani et al., 2017). Recently, KM has revealed that water exchange could be an indicator to measure microstructural characteristics in stroke patients (Lätt et al., 2009), developing brains or neurodegenerative diseases (Brusini et al., 2019; Olesen et al., 2022).

Note that, even though KM can be considered approximately valid in brain and muscle tissues (Fieremans et al., 2010), studies have found that KM fails in cases of rapid exchange (Fieremans et al., 2010; Nedjati-Gilani et al., 2017). Therefore, when KM is applied in processes involving rapid exchange, or applied to tissues with complex microstructures, the definition of multi-site exchange models seems ambiguous and needs careful discussion (Gardier et al., 2023).

4.2.2.3.1 TDKI

Diffusion kurtosis imaging (DKI) reveals the non-monotonic changes of kurtosis values in water exchange, which increase in the short-time domain and decrease in the long-time domain (Jensen et al., 2005; Jensen and Helpern, 2010). When the diffusion coefficient of the object under study does not change with time, indicating complete coarsening, it means that the applicable range of KM has been reached, and thus the water exchange time can be fitted from the time-dependent tail change of $K(t)$:

$$K(t)=K_0\cdot\frac{2\tau_{ex}}{t}\left[1-\frac{\tau_{ex}}{t}\left(1-e^{\frac{t}{\tau_{ex}}}\right)\right]+K_\infty, \qquad (8)$$

where K_0 represents the intrinsic kurtosis, and K_∞ signifies the situation where non-exchanging compartments remain.

This method has been applied to the measurement of water exchange in animal and human brain gray and white matter (Aggarwal et al., 2020; Lee et al., 2020b; Li et al., 2023), and tumor cells (Zhang et al., 2021; Solomon et al., 2023). Fig. 6 exhibits the example of TDKI application in breast tumor. When using the

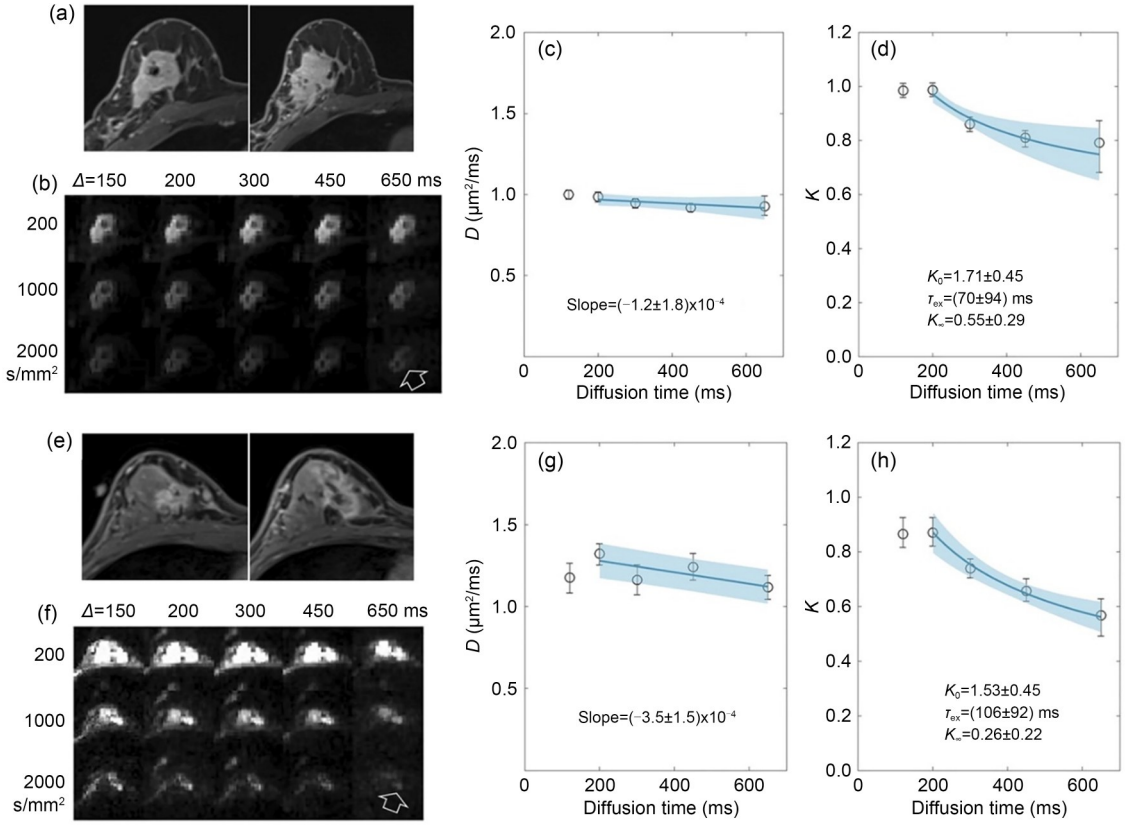

Fig. 6 TDKI data of two biopsy proven invasive ductal carcinomas in a 35-year-old woman (a–d) and a 56-year-old woman (e–h). In the long-time regime, $D(t)$ shows weak time dependency while $K(t)$ drops significantly. Reprinted from (Zhang et al., 2021), Copyright 2021, with permission from John Wiley and Sons

STEAM sequence, the complete coarsening time ($D(t)$ is time-invariant) for mouse gray matter structure is expected to be between 100 and 200 ms. In the study of Li et al. (2023), the exchange time for ex vivo mouse white matter was measured to be (232.4±16.0) ms (K_∞=0) and τ_{ex}=(17.6±10.5) ms (K_∞>0). Zhang et al. (2021) used a diffusion time of up to 800 ms to measure the exchange time in living mouse cortex bands, which was 30–40 ms. When using the PGSE sequence, the time dependency of $D(t)$ becomes very weak for animal and human gray matter when the diffusion time exceeds 20 ms. Jelescu et al. (2022) used the PGSE sequence to measure the exchange time in rat brain gray matter cortex in vivo in the range of 10–45 ms, which gave τ_{ex} = 16–21 ms (K_∞=0) and τ_{ex} = 0.4–0.9 ms (K_∞>0). Lee et al. (2020b) used the PGSE sequence to measure the exchange time in human brain gray matter in the range of 21–100 ms, which showed an estimated exchange time of about 11 ms. As for tumors, Zhang et al. (2021) measured τ_{ex} =68 ms in a mouse model of breast cancer and found similar exchange times (70 and 106 ms) in human experiments. Solomon et al. (2023) measured the water exchange time in clinical metastatic lymph nodes of head and neck cancer to be between 50 and 70 ms. The exchange times estimated in previous studies are listed in Table 2.

4.2.2.3.2 Combination of restriction and Karger model

One approach is to integrate the KM with multi-compartment models, specifying the two compartments of the KM as the intracellular (i.e., restricted) and extracellular (i.e., hindered) spaces. Sometimes a third compartment that does not participate in the exchange is added, considering the exchange between the intracellular and extracellular compartments, which better describes the phenomenon of water exchange existing in specific tissue structures such as brain gray matter, white matter, and tumors. NEXI (Jelescu et al., 2022), SANDIX, and SMEX (Olesen et al., 2022) have been used mainly in studies of brain gray and white matter. Jelescu et al. (2022) estimated the exchange time of living rat gray matter to be 12–20 ms. The JOINT model (Jiang et al., 2022) and CEXI model (Gardier et al., 2023) have been used mainly in studies of tumor tissues. Studies have involved performing simulation verification on the application of permeable limited sphere models and cell models, aiming to simultaneously measure cell size and transmembrane exchange information. Due to the requirements of higher b values (up to 10^4 s/mm^2) and shorter diffusion times, NEXI and CEXI have not yet been applied in human clinical practice. Recently, a model that can extend KM to any number of compartments has been proposed, using new indicators to explain water exchange (Jensen, 2024). A measurement strategy such as the free-gradient waveform has been developed to decouple restriction and exchange (Chakwizira et al., 2023). However, the gray and white matter structure of the brain is very complex. Taking into account the volume ratio of gray and white matter, differences in T1 and T2 relaxations, and the choice of diffusion time and sequence, estimates of water exchange time in different studies vary greatly. Even with the same model, different sequence

Table 2 Application of transmembrane water exchange time estimation in different studies

ROI	Model	Exchange time (mean) (ms)	Reference
Animal brain gray matter	NEXI	22	Jelescu et al., 2022
	TDKI (K_∞=0)	21	Jelescu et al., 2022
	TDKI (K_∞>0)	0.4	Jelescu et al., 2022
	TDKI (K_∞>0)	41	Zhang et al., 2021
Animal brain white matter	NEXI	105	Jelescu et al., 2022
	TDKI (K_∞=0)	232.4	Li et al., 2023
	TDKI (K_∞>0)	17.1	Li et al., 2023
Animal tumor	TDKI (K_∞>0)	68 and 93 (breast cancer)	Zhang et al., 2021
Human brain gray matter	TDKI (K_∞>0)	11	Lee et al., 2020b
	TDKI (K_∞=0)	250	Lee et al., 2020b
	Cumulant expansions	135	Chakwizira et al., 2023
Human brain gray matter	Cumulant expansions	285	Chakwizira et al., 2023
Human cerebellar gray matter	Cumulant expansions	115	Chakwizira et al., 2023
Human tumor	TDKI (K_∞>0)	50–70 (head and neck cancer), 88 (breast cancer)	Solomon et al., 2023

parameters can yield different estimates. For example, in the four datasets used in NEXI, the water exchange time for the cortex changes in the range of 10–60 ms (Jelescu et al., 2022). Numerous studies have demonstrated the potential for exchange between multiple compartments in the gray matter and the confounding effects of microstructures, but there is a lack of histological verification for the measurement values of water exchange and an urgent need for appropriate optimization solutions to bring these models into clinical application. The activity of water exchange reflected by the water exchange time may reflect the activity of tumor cells, the level of myelination, and the acute cell swelling and final membrane breakdown after ischemic stroke and disease processes. Thus, it is critical in studies of etiology and disease mechanisms of tumors and brain diseases, early diagnosis, and monitoring progress changes in the process of drug development.

5 Future developments

5.1 Hardware and acquisition

The extension of the diffusion time spectrum depends on the implementation of OGSE with higher frequencies and b values. Because $b \sim G^3/f^2$ (Xu, 2021), a stronger maximum gradient strength G_{max} and faster slew rate are required to achieve a higher frequency f while maintaining a reasonable b value. Over the past twenty years, the development of high gradient technology has propelled the whole-body gradient system of mainstream clinical superconducting magnetic resonance scanners from a G_{max} of about 40 mT/m and $R_{s,max}$ of about 200 T/(m·s) to 240 mT/m and 200 T/(m·s), respectively (United Imaging uMR Sagitta). In addition, the coil performance of the ultra-high gradient MRI system for head imaging has been increased to G_{max}= 650 mT/m and $R_{s,max}$=600 T/(m·s). Under this system, the highest frequency f of OGSE can theoretically reach 250 Hz (t_d=1 ms) while keeping b=500 s/mm^2. High-performance gradient systems can further enhance dMRI contrast and improve microstructural estimation accuracy (Wu et al., 2024).

Acquisition needs to be further improved to avoid undesired effects in the process. For instance, in current in vivo human studies, the use of OGSE in whole-body gradient systems is generally limited to relatively low b values and/or oscillation frequencies. To avoid signal attenuation caused by microcirculation flow at low b values, Wu and Zhang (2017) developed the DEFOG (diffusion encoding with dual-frequency orthogonal gradients) method. Some studies have also found that the effective spoiling gradient in the STEAM sequence (responsible for shattering the remnant magnetization after storage) may affect the theoretical diffusion time at long t_m (Kleinnijenhuis et al., 2018; Solomon et al., 2023). Additionally, while it avoids T2 decay, the T1 decay effect in the STEAM sequence might also be a potential factor impacting the signal (Solomon et al., 2023).

5.2 Optimization of models

A model is a simplified sketch of reality that can describe only a few relevant features of a tissue when its assumptions are met. Therefore, the design of models needs to focus on the main estimation parameters and sensible design of each experiment (i.e., pulse sequences, protocol parameters, etc.) to provide the most meaningful biomarkers and contrast (Jelescu et al., 2020). For example, our understanding of brain gray matter has evolved from “soma affecting the power law” (Palombo et al., 2020) to “both soma and exchange affecting the power law” (Jelescu et al., 2022).

The model fitting strategy is a critical factor to consider when assessing a model’s suitability for clinical applications. If a model includes too many free parameters, it may encounter difficulties during fitting. Given the presence of inevitable noise and artifacts in clinical scan data, it is essential to develop fitting algorithms that enhance accuracy, robustness, and efficiency. The use of techniques such as accelerated microstructure imaging via convex optimization (AMICO), machine learning, and deep learning networks has significantly enhanced the effectiveness of model fitting (Nedjati-Gilani et al., 2017; Bonet-Carne et al., 2019; Wu et al., 2023; Zheng et al., 2023).

Model validation requires histological inspection. Unfortunately, some models, such as water exchange, cannot obtain reliable histological validation (Lee et al., 2020b; Zhang et al., 2021; Li et al., 2023). Numerical models complement physical models as they provide a controlled and flexible tool to simulate how different mechanisms, such as diffusion, exchange, relaxation, and susceptibility changes, affect the magnetic resonance signal in a given microstructural geometry. The development of simulation models (Hwang et al.,

2003; Cook et al., 2005; Xu et al., 2007; Lee et al., 2021) and phantoms (Solomon et al., 2023; Xu et al., 2023) have greatly fostered the validation of models.

The development of models normally aims at generating quantitative biophysically specific imaging biomarkers. Numerous novel models and associated biomarkers have been proposed and used in disease diagnosis, prognosis, and various other domains (Table 1). However, despite these advancements, there remains a lack of multicenter validation, and the establishment of a universally acknowledged clinical application for microstructural maps remains elusive. Additionally, some techniques yield inconsistent, poorly understood, or contradictory outcomes, such as variations in water exchange time measurements across different models and discrepancies in axon diameter assessments. Hence, there is a pressing need for revolutionary modeling and validation studies, coupled with meticulous attention to calibration and reproducibility, to fully harness the potential of non-invasive three-dimensional intravital microstructural mapping (Novikov et al., 2018).

5.3 Clinical translation

dMRI lacks standardization. For example, in the diagnosis and treatment of breast cancer, the relationship between the ADC value and b value selections has been widely recognized (Baltzer et al., 2020), solving the problem of significant differences in ADC value results from different reports (Iima et al., 2020b). However, diffusion time is still a forgotten parameter, yet has a tremendous impact (Iima et al., 2021). Some studies have reported that different measurement times can cause up to 15% differences in ADC values (Someya et al., 2022), and in an extreme case, ADC could increase at long diffusion time but decrease at short diffusion time after treatments (Xu et al., 2012). The same problem also occurs in the diagnosis of other diseases. The standardization of diffusion time is also an important issue.

To apply in vivo microstructure imaging to cancer patients, the acquisition time must be tolerable, for example, about 10 min or less, as other anatomical and physiological images must be acquired from the same imaging process (Cao et al., 2024). For diseases like stroke that require urgent treatment, the patient's collection time needs to be even shorter. How to reduce collection time and ensure richer structural information puts high demands on the design of models and fitting algorithms.

6 Conclusions

There have been significant advances in TDDMRI research, with the technique gaining increased recognition as a powerful tool for revealing the microstructure of tissues. Advances in hardware, sequence designs, and the development of various mathematical models and computational methods have significantly enabled its application in diverse areas. From basic research to applications in early disease diagnosis, TDDMRI has shown great potential. However, there remain challenges to overcome. We must push for more efficient scanning and data processing technologies, develop accurate models to better describe and quantify the time-dependent behavior of molecular diffusion, and strive to develop more clinical application scenarios. Attention to these measures will ensure that this technology continues to evolve and provide invaluable insights into molecular diffusion in biological systems.

Acknowledgments

This work is supported by the Ministry of Science and Technology of the People's Republic of China (No. 2021ZD0200202), the National Natural Science Foundation of China (No. 82122032), and the Science and Technology Department of Zhejiang Province (Nos. 202006140 and 2022C03057).

Author contributions

Ruicheng BA and Dan WU designed the research and processed the corresponding data. Ruicheng BA wrote the first draft of the manuscript. Ruicheng BA, Liyi KANG, and Dan WU revised and edited the final version.

Conflict of interest

Ruicheng BA, Liyi KANG, and Dan WU declare that they have no conflict of interest.

References

Aggarwal M, Jones MV, Calabresi PA, et al., 2012. Probing mouse brain microstructure using oscillating gradient diffusion MRI. *Magnetic Resonance in Medicine*, 67(1): 98-109. https://doi.org/10.1002/mrm.22981

Aggarwal M, Burnsed J, Martin LJ, et al., 2014. Imaging neurodegeneration in the mouse hippocampus after neonatal hypoxia–ischemia using oscillating gradient diffusion MRI. *Magnetic Resonance in Medicine*, 72(3):829-840. https://doi.org/10.1002/mrm.24956

Aggarwal M, Smith MD, Calabresi PA, 2020. Diffusion-time dependence of diffusional kurtosis in the mouse brain. *Magnetic Resonance in Medicine*, 84(3):1564-1578. https://doi.org/10.1002/mrm.28189

Andrasko J, 1976. Water diffusion permeability of human erythrocytes studied by a pulsed gradient NMR technique. *Biochimica et Biophysica Acta (BBA)-General Subjects*, 428(2):304-311. https://doi.org/10.1016/0304-4165(76)90038-6

Arbabi A, Kai J, Khan AR, et al., 2020. Diffusion dispersion imaging: mapping oscillating gradient spin-echo frequency dependence in the human brain. *Magnetic Resonance in Medicine*, 83(6):2197-2208. https://doi.org/10.1002/mrm.28083

Ba RC, Wang XX, Zhang ZL, et al., 2023. Diffusion-time dependent diffusion MRI: effect of diffusion-time on microstructural mapping and prediction of prognostic features in breast cancer. *European Radiology*, 33(9):6226-6237. https://doi.org/10.1007/s00330-023-09623-y

Bailey C, Collins DJ, Tunariu N, et al., 2018. Microstructure characterization of bone metastases from prostate cancer with diffusion MRI: preliminary findings. *Frontiers in Oncology*, 8:26. https://doi.org/10.3389/fonc.2018.00026

Baltzer P, Mann RM, Iima M, et al., 2020. Diffusion-weighted imaging of the breast—a consensus and mission statement from the EUSOBI international breast diffusion-weighted imaging working group. *European Radiology*, 30(3):1436-1450. https://doi.org/10.1007/s00330-019-06510-3

Baron CA, Beaulieu C, 2014. Oscillating gradient spin-echo (OGSE) diffusion tensor imaging of the human brain. *Magnetic Resonance in Medicine*, 72(3):726-736. https://doi.org/10.1002/mrm.24987

Baron CA, Kate M, Gioia L, et al., 2015. Reduction of diffusion-weighted imaging contrast of acute ischemic stroke at short diffusion times. *Stroke*, 46(8):2136-2141. https://doi.org/10.1161/strokeaha.115.008815

Bonet-Carne E, Johnston E, Daducci A, et al., 2019. VERDICT-AMICO: ultrafast fitting algorithm for non-invasive prostate microstructure characterization. *NMR in Biomedicine*, 32(1):e4019. https://doi.org/10.1002/nbm.4019

Bongers A, Hau E, Shen H, 2018. Short diffusion time diffusion-weighted imaging with oscillating gradient preparation as an early magnetic resonance imaging biomarker for radiation therapy response monitoring in glioblastoma: a preclinical feasibility study. *International Journal of Radiation Oncology · Biology · Physics*, 102(4):1014-1023. https://doi.org/10.1016/j.ijrobp.2017.12.280

Boonrod A, Hagiwara A, Hori M, et al., 2018. Reduced visualization of cerebral infarction on diffusion-weighted images with short diffusion times. *Neuroradiology*, 60(9):979-982. https://doi.org/10.1007/s00234-018-2065-6

Borsos KB, Tse DHY, Dubovan PI, et al., 2023. Tuned bipolar oscillating gradients for mapping frequency dispersion of diffusion kurtosis in the human brain. *Magnetic Resonance in Medicine*, 89(2):756-766. https://doi.org/10.1002/mrm.29473

Brusini L, Menegaz G, Nilsson M, 2019. Monte Carlo simulations of water exchange through myelin wraps: implications for diffusion MRI. *IEEE Transactions on Medical Imaging*, 38(6):1438-1445. https://doi.org/10.1109/TMI.2019.2894398

Budde MD, Frank JA, 2010. Neurite beading is sufficient to decrease the apparent diffusion coefficient after ischemic stroke. *Proceedings of the National Academy of Sciences of the United States of America*, 107(32):14472-14477. https://doi.org/10.1073/pnas.1004841107

Burcaw LM, Fieremans E, Novikov DS, 2015. Mesoscopic structure of neuronal tracts from time-dependent diffusion. *NeuroImage*, 114:18-37. https://doi.org/10.1016/j.neuroimage.2015.03.061

Cao Y, Davarani SN, You D, et al., 2024. In vivo microstructure imaging in oropharyngeal squamous cell carcinoma using the random walk with barriers model. *Journal of Magnetic Resonance Imaging*, 59(3):929-938. https://doi.org/10.1002/jmri.28831

Chakwizira A, Westin CF, Brabec J, et al., 2023. Diffusion MRI with pulsed and free gradient waveforms: effects of restricted diffusion and exchange. *NMR in Biomedicine*, 36(1):e4827. https://doi.org/10.1002/nbm.4827

Clark CA, Hedehus M, Moseley ME, 2001. Diffusion time dependence of the apparent diffusion tensor in healthy human brain and white matter disease. *Magnetic Resonance in Medicine*, 45(6):1126-1129. https://doi.org/10.1002/mrm.1149

Colvin DC, Yankeelov TE, Does MD, et al., 2008. New insights into tumor microstructure using temporal diffusion spectroscopy. *Cancer Research*, 68(14):5941-5947. https://doi.org/10.1158/0008-5472.CAN-08-0832

Colvin DC, Loveless ME, Does MD, et al., 2011. Earlier detection of tumor treatment response using magnetic resonance diffusion imaging with oscillating gradients. *Magnetic Resonance Imaging*, 29(3):315-323. https://doi.org/10.1016/j.mri.2010.10.003

Cook PA, Bai Y, Hall MG, et al., 2005. Camino: diffusion MRI reconstruction and processing. MICCAI Open-Source Workshop. https://doi.org/10.54294/fgfrtv

Dai EP, Zhu AT, Yang GK, et al., 2023. Frequency-dependent diffusion kurtosis imaging in the human brain using an oscillating gradient spin echo sequence and a high-performance head-only gradient. *NeuroImage*, 279:120328. https://doi.org/10.1016/j.neuroimage.2023.120328

Devan SP, Jiang XY, Luo GZ, et al., 2022. Selective cell size MRI differentiates brain tumors from radiation necrosis. *Cancer Research*, 82(19):3603-3613. https://doi.org/10.1158/0008-5472.CAN-21-2929

Does MD, Parsons EC, Gore JC, 2003. Oscillating gradient measurements of water diffusion in normal and globally ischemic rat brain. *Magnetic Resonance in Medicine*, 49(2):206-215. https://doi.org/10.1002/mrm.10385

Fieremans E, Novikov DS, Jensen JH, et al., 2010. Monte Carlo study of a two-compartment exchange model of diffusion. *NMR in Biomedicine*, 23(7):711-724. https://doi.org/10.1002/nbm.1577

Fieremans E, Lemberskiy G, Veraart J, et al., 2017. In vivo

measurement of membrane permeability and myofiber size in human muscle using time-dependent diffusion tensor imaging and the random permeable barrier model. *NMR in Biomedicine*, 30(3):e3612. https://doi.org/10.1002/nbm.3612

Fokkinga E, Hernandez-Tamames JA, Ianus A, et al., 2023. Advanced diffusion-weighted MRI for cancer microstructure assessment in body imaging, and its relationship with histology. *Journal of Magnetic Resonance Imaging*, in press. https://doi.org/10.1002/jmri.29144

Foo TKF, Tan ET, Vermilyea ME, et al., 2020. Highly efficient head-only magnetic field insert gradient coil for achieving simultaneous high gradient amplitude and slew rate at 3.0T (MAGNUS) for brain microstructure imaging. *Magnetic Resonance in Medicine*, 83(6):2356-2369. https://doi.org/10.1002/mrm.28087

Gao FS, Shen XX, Zhang HX, et al., 2021. Feasibility of oscillating and pulsed gradient diffusion MRI to assess neonatal hypoxia-ischemia on clinical systems. *Journal of Cerebral Blood Flow & Metabolism*, 41(6):1240-1250. https://doi.org/10.1177/0271678X20944353

Gardier R, Villarreal Haro JL, Canales-Rodríguez EJ, et al., 2023. Cellular exchange imaging (CEXI): evaluation of a diffusion model including water exchange in cells using numerical phantoms of permeable spheres. *Magnetic Resonance in Medicine*, 90(4):1625-1640. https://doi.org/10.1002/mrm.29720

Gore JC, Xu JZ, Colvin DC, et al., 2010. Characterization of tissue structure at varying length scales using temporal diffusion spectroscopy. *NMR in Biomedicine*, 23(7):745-756. https://doi.org/10.1002/nbm.1531

Grussu F, Ianuş A, Tur C, et al., 2019. Relevance of time-dependence for clinically viable diffusion imaging of the spinal cord. *Magnetic Resonance in Medicine*, 81(2):1247-1264. https://doi.org/10.1002/mrm.27463

Haddar H, Li JR, Schiavi S, 2016. Adapting the Kärger model to account for finite diffusion-encoding pulses in diffusion MRI. *IMA Journal of Applied Mathematics*, 81(5):779-794. https://doi.org/10.1093/imamat/hxw032

Hao SJ, Wan Y, Xia YQ, et al., 2018. Size-based separation methods of circulating tumor cells. *Advanced Drug Delivery Reviews*, 125:3-20. https://doi.org/10.1016/j.addr.2018.01.002

Harkins KD, Galons JP, Secomb TW, et al., 2009. Assessment of the effects of cellular tissue properties on ADC measurements by numerical simulation of water diffusion. *Magnetic Resonance in Medicine*, 62(6):1414-1422. https://doi.org/10.1002/mrm.22155

Hattori T, Yuasa T, Aoki S, et al., 2011. Altered microstructure in corticospinal tract in idiopathic normal pressure hydrocephalus: comparison with Alzheimer disease and Parkinson disease with dementia. *American Journal of Neuroradiology*, 32(9):1681-1687. https://doi.org/10.3174/ajnr.A2570

Herrera SL, Sheft M, Mercredi ME, et al., 2022. Axon diameter inferences in the human corpus callosum using oscillating gradient spin echo sequences. *Magnetic Resonance Imaging*, 85:64-70. https://doi.org/10.1016/j.mri.2021.10.014

Hwang SN, Chin CL, Wehrli FW, et al., 2003. An image-based finite difference model for simulating restricted diffusion. *Magnetic Resonance in Medicine*, 50(2):373-382. https://doi.org/10.1002/mrm.10536

Iima M, Yamamoto A, Kataoka M, et al., 2019. Time-dependent diffusion MRI to distinguish malignant from benign head and neck tumors. *Journal of Magnetic Resonance Imaging*, 50(1):88-95. https://doi.org/10.1002/jmri.26578

Iima M, Honda M, Sigmund EE, et al., 2020a. Diffusion MRI of the breast: current status and future directions. *Journal of Magnetic Resonance Imaging*, 52(1):70-90. https://doi.org/10.1002/jmri.26908

Iima M, Partridge SC, le Bihan D, 2020b. Six DWI questions you always wanted to know but were afraid to ask: clinical relevance for breast diffusion MRI. *European Radiology*, 30(5):2561-2570. https://doi.org/10.1007/s00330-019-06648-0

Iima M, Kataoka M, Honda M, et al., 2021. The rate of apparent diffusion coefficient change with diffusion time on breast diffusion-weighted imaging depends on breast tumor types and molecular prognostic biomarker expression. *Investigative Radiology*, 56(8):501-508. https://doi.org/10.1097/RLI.0000000000000766

Jelescu IO, Palombo M, Bagnato F, et al., 2020. Challenges for biophysical modeling of microstructure. *Journal of Neuroscience Methods*, 344:108861. https://doi.org/10.1016/j.jneumeth.2020.108861

Jelescu IO, de Skowronski A, Geffroy F, et al., 2022. Neurite exchange imaging (NEXI): a minimal model of diffusion in gray matter with inter-compartment water exchange. *NeuroImage*, 256:119277. https://doi.org/10.1016/j.neuroimage.2022.119277

Jensen JH, 2024. Diffusional kurtosis time dependence and the water exchange rate for the multi-compartment Kärger model. *Magnetic Resonance in Medicine*, 91(3):1122-1135. https://doi.org/10.1002/mrm.29926

Jensen JH, Helpern JA, 2010. MRI quantification of non-Gaussian water diffusion by kurtosis analysis. *NMR in Biomedicine*, 23(7):698-710. https://doi.org/10.1002/nbm.1518

Jensen JH, Helpern JA, Ramani A, et al., 2005. Diffusional kurtosis imaging: the quantification of non-Gaussian water diffusion by means of magnetic resonance imaging. *Magnetic Resonance in Medicine*, 53(6):1432-1440. https://doi.org/10.1002/mrm.20508

Jespersen SN, Olesen JL, Hansen B, et al., 2018. Diffusion time dependence of microstructural parameters in fixed spinal cord. *NeuroImage*, 182:329-342. https://doi.org/10.1016/j.neuroimage.2017.08.039

Jiang XY, Li H, Xie JP, et al., 2016. Quantification of cell size using temporal diffusion spectroscopy. *Magnetic Resonance in Medicine*, 75(3):1076-1085. https://doi.org/10.1002/mrm.25684

Jiang XY, Li H, Xie JP, et al., 2017. In vivo imaging of cancer cell size and cellularity using temporal diffusion spectroscopy. *Magnetic Resonance in Medicine*, 78(1):156-164. https://doi.org/10.1002/mrm.26356

Jiang XY, Xu JZ, Gore JC, 2019. Quantitative temporal diffusion spectroscopy as an early imaging biomarker of radiation therapeutic response in gliomas: a preclinical proof of concept. *Advances in Radiation Oncology*, 4(2):367-376. https://doi.org/10.1016/j.adro.2018.11.003

Jiang XY, Xu JZ, Gore JC, 2020a. Mapping hepatocyte size in vivo using temporal diffusion spectroscopy MRI. *Magnetic Resonance in Medicine*, 84(5):2671-2683. https://doi.org/10.1002/mrm.28299

Jiang XY, Dudzinski S, Beckermann KE, et al., 2020b. MRI of tumor T cell infiltration in response to checkpoint inhibitor therapy. *Journal for ImmunoTherapy of Cancer*, 8(1): e000328. https://doi.org/10.1136/jitc-2019-000328

Jiang XY, Li H, Devan SP, et al., 2021. MR cell size imaging with temporal diffusion spectroscopy. *Magnetic Resonance Imaging*, 77:109-123. https://doi.org/10.1016/j.mri.2020.12.010

Jiang XY, Devan SP, Xie JP, et al., 2022. Improving MR cell size imaging by inclusion of transcytolemmal water exchange. *NMR in Biomedicine*, 35(12):e4799. https://doi.org/10.1002/nbm.4799

Jiang XY, McKinley ET, Xie JP, et al., 2024. Detection of treatment response in triple-negative breast tumors to paclitaxel using MRI cell size imaging. *Journal of Magnetic Resonance Imaging*, 59(2):575-584. https://doi.org/10.1002/jmri.28774

Johnston E, Pye H, Bonet-Carne E, et al., 2016. INNOVATE: a prospective cohort study combining serum and urinary biomarkers with novel diffusion-weighted magnetic resonance imaging for the prediction and characterization of prostate cancer. *BMC Cancer*, 16(1):816. https://doi.org/10.1186/s12885-016-2856-2

Johnston E, Bonet-Carne E, Ferizi U, et al., 2019. VERDICT MRI for prostate cancer: intracellular volume fraction versus apparent diffusion coefficient. *Radiology*, 291(2): 391-397. https://doi.org/10.1148/radiol.2019181749

Kakkar LS, Bennett OF, Siow B, et al., 2018. Low frequency oscillating gradient spin-echo sequences improve sensitivity to axon diameter: an experimental study in viable nerve tissue. *NeuroImage*, 182:314-328. https://doi.org/10.1016/j.neuroimage.2017.07.060

Kamimura K, Kamimura Y, Nakano T, et al., 2023a. Differentiating brain metastasis from glioblastoma by time-dependent diffusion MRI. *Cancer Imaging*, 23(1):75. https://doi.org/10.1186/s40644-023-00595-2

Kamimura K, Nakano T, Hasegawa T, et al., 2023b. Differentiating primary central nervous system lymphoma from glioblastoma by time-dependent diffusion using oscillating gradient. *Cancer Imaging*, 23(1):114. https://doi.org/10.1186/s40644-023-00639-7

Kärger J, 1985. NMR self-diffusion studies in heterogeneous systems. *Advances in Colloid and Interface Science*, 23: 129-148. https://doi.org/10.1016/0001-8686(85)80018-X

Kärger J, Pfeifer H, Heink W, 1988. Principles and application of self-diffusion measurements by nuclear magnetic resonance. *Advances in Magnetic and Optical Resonance*, 12:1-89. https://doi.org/10.1016/B978-0-12-025512-2.50004-X

Kershaw J, Leuze C, Aoki I, et al., 2013. Systematic changes to the apparent diffusion tensor of in vivo rat brain measured with an oscillating-gradient spin-echo sequence. *NeuroImage*, 70:10-20. https://doi.org/10.1016/j.neuroimage.2012.12.036

Kleinnijenhuis M, Mollink J, Lam WW, et al., 2018. Choice of reference measurements affects quantification of long diffusion time behaviour using stimulated echoes. *Magnetic Resonance in Medicine*, 79(2):952-959. https://doi.org/10.1002/mrm.26711

Lätt J, Nilsson M, van Westen D, et al., 2009. Diffusion-weighted MRI measurements on stroke patients reveal water-exchange mechanisms in sub-acute ischaemic lesions. *NMR in Biomedicine*, 22(6):619-628. https://doi.org/10.1002/nbm.1376

Lee HH, Papaioannou A, Kim SL, et al., 2020a. A time-dependent diffusion MRI signature of axon caliber variations and beading. *Communications Biology*, 3(1):354. https://doi.org/10.1038/s42003-020-1050-x

Lee HH, Papaioannou A, Novikov DS, et al., 2020b. In vivo observation and biophysical interpretation of time-dependent diffusion in human cortical gray matter. *NeuroImage*, 222: 117054. https://doi.org/10.1016/j.neuroimage.2020.117054

Lee HH, Fieremans E, Novikov DS, 2021. Realistic microstructure simulator (RMS): Monte Carlo simulations of diffusion in three-dimensional cell segmentations of microscopy images. *Journal of Neuroscience Methods*, 350:109018. https://doi.org/10.1016/j.jneumeth.2020.109018

Lemberskiy G, Rosenkrantz AB, Veraart J, et al., 2017a. Time-dependent diffusion in prostate cancer. *Investigative Radiology*, 52(7):405-411. https://doi.org/10.1097/RLI.0000000000000356

Lemberskiy G, Baete SH, Cloos MA, et al., 2017b. Validation of surface-to-volume ratio measurements derived from oscillating gradient spin echo on a clinical scanner using anisotropic fiber phantoms. *NMR in Biomedicine*, 30(5): e3708. https://doi.org/10.1002/nbm.3708

Lemberskiy G, Fieremans E, Veraart J, et al., 2018. Characterization of prostate microstructure using water diffusion and NMR relaxation. *Frontiers in Physics*, 6:91. https://doi.org/10.3389/fphy.2018.00091

Lemberskiy G, Feiweier T, Gyftopoulos S, et al., 2021. Assessment of myofiber microstructure changes due to atrophy and recovery with time-dependent diffusion MRI. *NMR in Biomedicine*, 34(7):e4534. https://doi.org/10.1002/nbm.4534

Li CY, Fieremans E, Novikov DS, et al., 2023. Measuring water exchange on a preclinical MRI system using filter exchange and diffusion time dependent kurtosis imaging.

Magnetic Resonance in Medicine, 89(4):1441-1455. https://doi.org/10.1002/mrm.29536

Liu KY, Lin ZX, Zheng TS, et al., 2024. Improving microstructural estimation in time-dependent diffusion MRI with a Bayesian method. *Journal of Magnetic Resonance Imaging*, in press. https://doi.org/10.1002/jmri.29434

Maekawa T, Hori M, Murata K, et al., 2019. Choroid plexus cysts analyzed using diffusion-weighted imaging with short diffusion-time. *Magnetic Resonance Imaging*, 57:323-327. https://doi.org/10.1016/j.mri.2018.12.010

Maekawa T, Hori M, Murata K, et al., 2020. Differentiation of high-grade and low-grade intra-axial brain tumors by time-dependent diffusion MRI. *Magnetic Resonance Imaging*, 72:34-41. https://doi.org/10.1016/j.mri.2020.06.018

Maekawa T, Hori M, Murata K, et al., 2023. Investigation of time-dependent diffusion in extra-axial brain tumors using oscillating-gradient spin-echo. *Magnetic Resonance Imaging*, 96:67-74. https://doi.org/10.1016/j.mri.2022.11.010

McDowell AR, Feiweier T, Muntoni F, et al., 2021. Clinically feasible diffusion MRI in muscle: time dependence and initial findings in Duchenne muscular dystrophy. *Magnetic Resonance in Medicine*, 86(6):3192-3200. https://doi.org/10.1002/mrm.28945

Meier C, Dreher W, Leibfritz D, 2003. Diffusion in compartmental systems. I. A comparison of an analytical model with simulations. *Magnetic Resonance in Medicine*, 50(3):500-509. https://doi.org/10.1002/mrm.10557

Merboldt KD, Hänicke W, Frahm J, 1991. Diffusion imaging using stimulated echoes. *Magnetic Resonance in Medicine*, 19(2):233-239. https://doi.org/10.1002/mrm.1910190208

Mitra PP, Sen PN, Schwartz LM, et al., 1992. Diffusion propagator as a probe of the structure of porous media. *Physical Review Letters*, 68(24):3555-3558. https://doi.org/10.1103/PhysRevLett.68.3555

Mitra PP, Sen PN, Schwartz LM, 1993. Short-time behavior of the diffusion coefficient as a geometrical probe of porous media. *Physical Review B*, 47(14):8565-8574. https://doi.org/10.1103/physrevb.47.8565

Nedjati-Gilani GL, Schneider T, Hall MG, et al., 2017. Machine learning based compartment models with permeability for white matter microstructure imaging. *NeuroImage*, 150:119-135. https://doi.org/10.1016/j.neuroimage.2017.02.013

Nilsson M, Lätt J, Nordh E, et al., 2009. On the effects of a varied diffusion time in vivo: is the diffusion in white matter restricted? *Magnetic Resonance Imaging*, 27(2):176-187. https://doi.org/10.1016/j.mri.2008.06.003

Novikov DS, Kiselev VG, 2011. Surface-to-volume ratio with oscillating gradients. *Journal of Magnetic Resonance*, 210(1):141-145. https://doi.org/10.1016/j.jmr.2011.02.011

Novikov DS, Fieremans E, Jensen JH, et al., 2011. Random walks with barriers. *Nature Physics*, 7(6):508-514. https://doi.org/10.1038/nphys1936

Novikov DS, Jensen JH, Helpern JA, et al., 2014. Revealing mesoscopic structural universality with diffusion. *Proceedings of the National Academy of Sciences of the United States of America*, 111(14):5088-5093. https://doi.org/10.1073/pnas.1316944111

Novikov DS, Kiselev VG, Jespersen SN, 2018. On modeling. *Magnetic Resonance in Medicine*, 79(6):3172-3193. https://doi.org/10.1002/mrm.27101

Novikov DS, Fieremans E, Jespersen SN, et al., 2019. Quantifying brain microstructure with diffusion MRI: theory and parameter estimation. *NMR in Biomedicine*, 32(4):e3998. https://doi.org/10.1002/nbm.3998

Olesen JL, Østergaard L, Shemesh N, et al., 2022. Diffusion time dependence, power-law scaling, and exchange in gray matter. *NeuroImage*, 251:118976. https://doi.org/10.1016/j.neuroimage.2022.118976

Palombo M, Ianus A, Guerreri M, et al., 2020. SANDI: a compartment-based model for non-invasive apparent soma and neurite imaging by diffusion MRI. *NeuroImage*, 215:116835. https://doi.org/10.1016/j.neuroimage.2020.116835

Palombo M, Valindria V, Singh S, et al., 2023. Joint estimation of relaxation and diffusion tissue parameters for prostate cancer with relaxation-VERDICT MRI. *Scientific Reports*, 13(1):2999. https://doi.org/10.1038/s41598-023-30182-1

Panagiotaki E, Walker-Samuel S, Siow B, et al., 2014. Noninvasive quantification of solid tumor microstructure using VERDICT MRI. *Cancer Research*, 74(7):1902-1912. https://doi.org/10.1158/0008-5472.CAN-13-2511

Panagiotaki E, Chan RW, Dikaios N, et al., 2015. Microstructural characterization of normal and malignant human prostate tissue with vascular, extracellular, and restricted diffusion for cytometry in tumours magnetic resonance imaging. *Investigative Radiology*, 50(4):218-227. https://doi.org/10.1097/RLI.0000000000000115

Paran Y, Bendel P, Margalit R, et al., 2004. Water diffusion in the different microenvironments of breast cancer. *NMR in Biomedicine*, 17(4):170-180. https://doi.org/10.1002/nbm.882

Parsons EC, Does MD, Gore JC, 2003. Modified oscillating gradient pulses for direct sampling of the diffusion spectrum suitable for imaging sequences. *Magnetic Resonance Imaging*, 21(3-4):279-285. https://doi.org/10.1016/S0730-725X(03)00155-3

Parsons Jr EC, Does MD, Gore JC, 2006. Temporal diffusion spectroscopy: theory and implementation in restricted systems using oscillating gradients. *Magnetic Resonance in Medicine*, 55(1):75-84. https://doi.org/10.1002/mrm.20732

Price WS, Barzykin AV, Hayamizu K, et al., 1998. A model for diffusive transport through a spherical interface probed by pulsed-field gradient NMR. *Biophysical Journal*, 74(5):2259-2271. https://doi.org/10.1016/S0006-3495(98)77935-4

Reynaud O, 2017. Time-dependent diffusion MRI in cancer:

tissue modeling and applications. *Frontiers in Physics*, 5:58. https://doi.org/10.3389/fphy.2017.00058

Reynaud O, Winters KV, Hoang DM, et al., 2016. Pulsed and oscillating gradient MRI for assessment of cell size and extracellular space (POMACE) in mouse gliomas. *NMR in Biomedicine*, 29(10):1350-1363. https://doi.org/10.1002/nbm.3577

Saliani A, Perraud B, Duval T, et al., 2017. Axon and myelin morphology in animal and human spinal cord. *Frontiers in Neuroanatomy*, 11:129. https://doi.org/10.3389/fnana.2017.00129

Schachter M, Does MD, Anderson AW, et al., 2000. Measurements of restricted diffusion using an oscillating gradient spin-echo sequence. *Journal of Magnetic Resonance*, 147(2):232-237. https://doi.org/10.1006/jmre.2000.2203

Shi RY, Yao QY, Wu LM, et al., 2018. Breast lesions: diagnosis using diffusion weighted imaging at 1.5T and 3.0T—systematic review and meta-analysis. *Clinical Breast Cancer*, 18(3):e305-e320. https://doi.org/10.1016/j.clbc.2017.06.011

Sigmund EE, Novikov DS, Sui D, et al., 2014. Time-dependent diffusion in skeletal muscle with the random permeable barrier model (RPBM): application to normal controls and chronic exertional compartment syndrome patients. *NMR in Biomedicine*, 27(5):519-528. https://doi.org/10.1002/nbm.3087

Singh S, Rogers H, Kanber B, et al., 2022. Avoiding unnecessary biopsy after multiparametric prostate MRI with VERDICT analysis: the INNOVATE study. *Radiology*, 305(3):623-630. https://doi.org/10.1148/radiol.212536

Solomon E, Lemberskiy G, Baete S, et al., 2023. Time-dependent diffusivity and kurtosis in phantoms and patients with head and neck cancer. *Magnetic Resonance in Medicine*, 89(2):522-535. https://doi.org/10.1002/mrm.29457

Someya Y, Iima M, Imai H, et al., 2022. Investigation of breast cancer microstructure and microvasculature from time-dependent DWI and CEST in correlation with histological biomarkers. *Scientific Reports*, 12(1):6523. https://doi.org/10.1038/s41598-022-10081-7

Stanisz GJ, Li JG, Wright GA, et al., 1998. Water dynamics in human blood via combined measurements of T_2 relaxation and diffusion in the presence of gadolinium. *Magnetic Resonance in Medicine*, 39(2):223-233. https://doi.org/10.1002/mrm.1910390209

Stejskal EO, Tanner JE, 1965. Spin diffusion measurements: spin echoes in the presence of a time-dependent field gradient. *The Journal of Chemical Physics*, 42(1):288-292. https://doi.org/10.1063/1.1695690

Tan ET, Shih RY, Mitra J, et al., 2020. Oscillating diffusion-encoding with a high gradient-amplitude and high slew-rate head-only gradient for human brain imaging. *Magnetic Resonance in Medicine*, 84(2):950-965. https://doi.org/10.1002/mrm.28180

Tanner JE, 1983. Intracellular diffusion of water. *Archives of Biochemistry and Biophysics*, 224(2):416-428. https://doi.org/10.1016/0003-9861(83)90228-X

Tétreault P, Harkins KD, Baron CA, et al., 2020. Diffusion time dependency along the human corpus callosum and exploration of age and sex differences as assessed by oscillating gradient spin-echo diffusion tensor imaging. *NeuroImage*, 210:116533. https://doi.org/10.1016/j.neuroimage.2020.116533

Van AT, Holdsworth SJ, Bammer R, 2014. In vivo investigation of restricted diffusion in the human brain with optimized oscillating diffusion gradient encoding. *Magnetic Resonance in Medicine*, 71(1):83-94. https://doi.org/10.1002/mrm.24632

Wagner M, Doblas S, Poté N, et al., 2020. Comparison of pulsed and oscillating gradient diffusion-weighted MRI for characterizing hepatocellular nodules in liver cirrhosis: ex vivo study in a rat model. *Journal of Magnetic Resonance Imaging*, 51(4):1065-1074. https://doi.org/10.1002/jmri.26919

Warach S, Gaa J, Siewert B, et al., 1995. Acute human stroke studied by whole brain echo planar diffusion-weighted magnetic resonance imaging. *Annals of Neurology*, 37(2):231-241. https://doi.org/10.1002/ana.410370214

Winters KV, Reynaud O, Novikov DS, et al., 2018. Quantifying myofiber integrity using diffusion MRI and random permeable barrier modeling in skeletal muscle growth and Duchenne muscular dystrophy model in mice. *Magnetic Resonance in Medicine*, 80(5):2094-2108. https://doi.org/10.1002/mrm.27188

Wu D, Zhang JY, 2017. The effect of microcirculatory flow on oscillating gradient diffusion MRI and diffusion encoding with dual-frequency orthogonal gradients (DEFOG). *Magnetic Resonance in Medicine*, 77(4):1583-1592. https://doi.org/10.1002/mrm.26242

Wu D, Martin LJ, Northington FJ, et al., 2014. Oscillating gradient diffusion MRI reveals unique microstructural information in normal and hypoxia-ischemia injured mouse brains. *Magnetic Resonance in Medicine*, 72(5):1366-1374. https://doi.org/10.1002/mrm.25441

Wu D, Li Q, Northington FJ, et al., 2018. Oscillating gradient diffusion kurtosis imaging of normal and injured mouse brains. *NMR in Biomedicine*, 31(6):e3917. https://doi.org/10.1002/nbm.3917

Wu D, Martin LJ, Northington FJ, et al., 2019. Oscillating-gradient diffusion magnetic resonance imaging detects acute subcellular structural changes in the mouse forebrain after neonatal hypoxia-ischemia. *Journal of Cerebral Blood Flow & Metabolism*, 39(7):1336-1348. https://doi.org/10.1177/0271678X18759859

Wu D, Kang LY, Li HT, et al., 2024. Developing an AI-empowered head-only ultra-high-performance gradient MRI system for high spatiotemporal neuroimaging. *NeuroImage*, 290:120553. https://doi.org/10.1016/j.neuroimage.2024.120553

Wu J, Kang TS, Lan XL, et al., 2023. IMPULSED model based cytological feature estimation with U-Net: application to human brain tumor at 3T. *Magnetic Resonance in Medicine*, 89(1):411-422.

https://doi.org/10.1002/mrm.29429

Xu JZ, 2021. Probing neural tissues at small scales: recent progress of oscillating gradient spin echo (OGSE) neuroimaging in humans. *Journal of Neuroscience Methods*, 349: 109024.
https://doi.org/10.1016/j.jneumeth.2020.109024

Xu JZ, Does MD, Gore JC, 2007. Numerical study of water diffusion in biological tissues using an improved finite difference method. *Physics in Medicine & Biology*, 52(7): N111-N126.
https://doi.org/10.1088/0031-9155/52/7/n01

Xu JZ, Xie JP, Jourquin J, et al., 2011. Influence of cell cycle phase on apparent diffusion coefficient in synchronized cells detected using temporal diffusion spectroscopy. *Magnetic Resonance in Medicine*, 65(4):920-926.
https://doi.org/10.1002/mrm.22704

Xu JZ, Li K, Smith RA, et al., 2012. Characterizing tumor response to chemotherapy at various length scales using temporal diffusion spectroscopy. *PLoS One*, 7(7):e41714.
https://doi.org/10.1371/journal.pone.0041714

Xu JZ, Li H, Harkins KD, et al., 2014. Mapping mean axon diameter and axonal volume fraction by MRI using temporal diffusion spectroscopy. *NeuroImage*, 103:10-19.
https://doi.org/10.1016/j.neuroimage.2014.09.006

Xu JZ, Jiang XY, Li H, et al., 2020. Magnetic resonance imaging of mean cell size in human breast tumors. *Magnetic Resonance in Medicine*, 83(6):2002-2014.
https://doi.org/10.1002/mrm.28056

Xu JZ, Jiang XY, Devan SP, et al., 2021. MRI-cytometry: mapping nonparametric cell size distributions using diffusion MRI. *Magnetic Resonance in Medicine*, 85(2):748-761.
https://doi.org/10.1002/mrm.28454

Xu JZ, Xie JP, Semmineh NB, et al., 2023. Diffusion time dependency of extracellular diffusion. *Magnetic Resonance in Medicine*, 89(6):2432-2440.
https://doi.org/10.1002/mrm.29594

Zhang HX, Liu KY, Ba RC, et al., 2023. Histological and molecular classifications of pediatric glioma with time-dependent diffusion MRI-based microstructural mapping. *Neuro-Oncology*, 25(6):1146-1156.
https://doi.org/10.1093/neuonc/noad003

Zhang J, Lemberskiy G, Moy L, et al., 2021. Measurement of cellular-interstitial water exchange time in tumors based on diffusion-time-dependent diffusional kurtosis imaging. *NMR in Biomedicine*, 34(6):e4496.
https://doi.org/10.1002/nbm.4496

Zheng TS, Ba RC, Wang XL, et al., 2023. AUA-dE: an adaptive uncertainty guided attention for diffusion MRI models estimation. Proceedings of the 26th International Conference on Medical Image Computing and Computer Assisted Intervention, p.142-151.
https://doi.org/10.1007/978-3-031-43993-3_14

Zhu AT, Shih R, Huang RY, et al., 2023. Revealing tumor microstructure with oscillating diffusion encoding MRI in presurgical and post-treatment glioma patients. *Magnetic Resonance in Medicine*, 90(5):1789-1801.
https://doi.org/10.1002/mrm.29758